Mapping the immunogenic landscape of near-native HIV-1 envelope trimers in non-human primates

Christopher A. Cottrell[1,2,3], Jelle van Schooten[4], Charles A. Bowman[1], Meng Yuan[1], David Oyen[1], Mia Shin[1], Robert Morpurgo[4], Patricia van der Woude[4], Marielle van Breemen[4], Jonathan L. Torres[1], Raj Patel[1], Justin Gross[1], Leigh M. Sewall[1], Jeffrey Copps[1], Gabriel Ozorowski[1,2,3], Bartek Nogal[1,2,3], Devin Sok[2,3,5], Eva G. Rakasz[6], Celia Labranche[7], Vladimir Vigdorovich[12], Scott Christley[13], Diane G. Carnathan[3,14], D. Noah Sather[12], David Montefiori[7,8], Guido Silvestri[3,14], Dennis R. Burton[2,3,5,9], John P. Moore[10], Ian A. Wilson[1,2,3,11], Rogier W. Sanders[1,10#], Andrew B. Ward[1,2,3#], Marit J. van Gils[4#]

[1] Department of Integrative Structural and Computational Biology, The Scripps Research Institute, La Jolla, CA 92037, USA.

[2] IAVI Neutralizing Antibody Center, The Scripps Research Institute, La Jolla, CA 92037, USA.

[3] Consortium for HIV/AIDS Vaccine Development, The Scripps Research Institute, La Jolla, CA 92037, USA.

[4] Department of Medical Microbiology, Amsterdam UMC, University of Amsterdam, 1105 AZ Amsterdam, The Netherlands.

[5] Department of Immunology and Microbiology, The Scripps Research Institute, La Jolla, CA 92037, USA.

[6] Wisconsin National Primate Research Center, University of Wisconsin, Madison, WI 53715, USA.

[7] Department of Surgery, Duke University Medical Center, Durham, NC 27710, USA.

[8] Duke Human Vaccine Institute, Duke University Medical Center, Durham, NC 27710, USA.

[9] The Ragon Institute of Massachusetts General Hospital, Massachusetts Institute of Technology and Harvard University, Cambridge, MA 02139, USA.

[10] Department of Microbiology and Immunology, Weill Medical College of Cornell University, New York, NY 10021,USA

[11] The Skaggs Institute for Chemical Biology, The Scripps Institute, La Jolla, CA 92037, USA

[12] Center for Global Infectious Disease Research, Seattle Children's Research Institute, Seattle, WA 98109, USA.

[13] Department of Population and Data Sciences, UT Southwestern Medical Center, Dallas, TX 75390, USA

[14] Yerkes National Primate Research Center, Emory University, Atlanta, GA 30322, USA;

[#] corresponding author; m.j.vangils@amc.uva.nl; andrew@scripps.edu; r.w.sanders@amc.uva.nl

Summary

The induction of broad and potent immunity by vaccines is the key focus of research efforts aimed at protecting against HIV-1 infection. Soluble native-like HIV-1 envelope glycoproteins have shown promise as vaccine candidates as they can induce potent autologous neutralizing responses in rabbits and non-human primates. In this study, monoclonal antibodies were isolated and characterized from rhesus macaques immunized with the BG505 SOSIP.664 trimer to better understand vaccine-induced antibody responses. Our studies reveal a diverse landscape of antibodies recognizing immunodominant strain-specific epitopes and non-neutralizing neo-epitopes. Additionally, we isolated a subset of mAbs against an epitope cluster at the gp120-gp41 interface that recognize the highly conserved fusion peptide and the glycan at position 88 and have characteristics akin to several human-derived broadly neutralizing antibodies.

Introduction

HIV-1 continues to cause significant morbidity and mortality around the world with an estimated 1.7 million new infections in 2018 (UNAIDS, 2019), which emphasizes the need for an effective prophylactic vaccine. The HIV-1 envelope glycoprotein (Env) is the sole target for neutralizing antibody (NAb) responses. Studies of infected patients have led to the isolation of NAbs against multiple different epitopes on the Env surface that are capable of both neutralizing most circulating strains and providing passive protection against repeated viral challenges in non-human primates (NHPs) (Burton and Hangartner, 2016; Moldt et al., 2016; Pegu et al., 2019; Wu, 2018). Extensive research efforts, including structure-based engineering of Env immunogens, are currently directed towards developing vaccine strategies to successfully elicit broadly neutralizing antibodies (bNAbs) against specific Env epitopes (de Taeye et al., 2015; Escolano et al., 2019; Escolano et al., 2016; Jardine et al., 2016; Kong et al., 2019; Steichen et al., 2016; Torrents de la Pena et al., 2017). The development and structural determination of soluble native-like Env trimer mimics, particularly ones based on the SOSIP technology, has provided a platform for structure-based immunogen design (Julien et al., 2013a; Lyumkis et al., 2013; Pancera et al., 2014; Sanders et al., 2013). NAbs induced by SOSIP trimers in NHPs can protect against challenge with an autologous Simian-Human Immunodeficiency virus (SHIV) (Pauthner et al., 2017; Pauthner et al., 2019). However, as NAbs with the required breadth of activity have not yet been induced in trimer-immunized animals, improvements to current vaccine design and delivery strategies are clearly needed.

Characterizing the antibody response to SOSIP trimers may provide useful information for guiding immunogen design. Initial analyses of rabbits immunized with BG505 SOSIP.664 trimers,

including studies of isolated monoclonal antibodies (mAbs), showed that autologous NAbs targeted a large hole in the glycan shield of the BG505 virus caused by the absence of glycosylation sites at positions 241 and 289 (Klasse et al., 2018; McCoy et al., 2016). The 241 glycan is highly conserved (97%) among HIV-1 strains and while the 289 glycan is less conserved, it is still present in 79% of viruses. The required absence of typically conserved glycans explains why the NAbs isolated from the trimer-immunized rabbits lack breadth (McCoy et al., 2016). Later studies involving BG505 trimer-immunized rabbits, guinea pigs, and NHPs have identified additional narrow-specificity neutralizing serum responses that recognize epitopes in the C3/V4, C3/V5, and V1 regions, with mAbs isolated from guinea pigs targeting the C3/V4 epitope (Cirelli et al., 2019; Klasse et al., 2018; Lei et al., 2019; Nogal et al., 2019; Pauthner et al., 2017).

Here, we describe a detailed characterization of neutralizing and non-neutralizing mAbs isolated from two rhesus macaques (RMs) previously immunized with the BG505 SOSIP.664 trimer (Sanders et al., 2015). We identified multiple mAbs targeting the 289-glycan hole on the BG505 SOSIP.664 trimer or a neo-epitope cluster at the base of the trimer. The most potent NAb isolated targeted the gp120/gp41 interface at an epitope that significantly overlaps with the epitope of human bNAb VRC34 (Kong et al., 2016). Insights from the induction of these NAbs through vaccination can be further used to develop immunogens and immunization strategies to induce cross-reactive antibody responses.

Results

Indian origin rhesus macaque BCR germline database

The majority of bNAbs isolated from HIV-infected patients have exceedingly high levels of somatic hypermutation (SHM) (Landais and Moore, 2018; Wu, 2018). Accurately measuring levels of SHM elicited during immunization experiments is a critical component to ensuring the elicited antibodies are acquiring the level of mutations associated with neutralization breadth. To accurately measure the extent of SHM, the mAb sequences that we obtained from BG505 SOSIP.664 trimer-immunized RMs required comparison to a germline B-cell receptor (BCR) reference database. The IMGT reference database for RMs is incomplete and contains a mixture of genes/alleles from both Chinese and Indian origin animals. Given the high levels of genetic diversity in the Immunoglobulin (Ig) loci among RMs from different origins (Corcoran et al., 2016) and the general use of Indian origin RMs in most HIV-1 immunization experiments conducted in the United States, we constructed a germline database containing gene/alleles from only Indian origin RMs. The gene/alleles from the published database (Vigdorovich et al., 2016) were aligned to the Mmul_8.0.1 Indian origin RM genome assembly using BLAST (Johnson et al., 2008; Zimin et al., 2014). Sequences that were not identical to the reference genome were eliminated. Additional genes/alleles from publicly available Indian origin RM genomic DNA sequencing datasets (Cirelli et al., 2019; Ramesh et al., 2017) were added to the database. After duplicates were removed, the resulting new database contained 189 IGHV, 70 IGHD, 9 IGHJ, 188 IGKV, 5 IGKJ, 147 IGLV, and 13 IGLJ genes/alleles (Table S1).

Recent advances in BCR repertoire sequencing and analysis have enabled the use of next-generation sequencing (NGS) datasets for inferring novel genes/alleles (Corcoran et al., 2016;

Gadala-Maria et al., 2015; Ralph and Matsen, 2018). Using the database described above as an initial database, we performed IgDiscover analysis (Corcoran et al., 2016) on IgM BCR sequences derived from five Indian origin RMs. Additionally, we performed IgDiscover analysis on previously obtained Indian origin RM BCR NGS datasets that were downloaded from the NCBI sequence read archive (Corcoran et al., 2016; Guo et al., 2015) or obtained directly from the study authors (Vigdorovich et al., 2016). Inferred genes/alleles were kept if they were detected in more than one animal or if they were identical to RM genes/alleles that were previously deposited in the NCBI database. We added 113 IGHV, 18 IGKV, and 18 IGLV genes/alleles to our germline database (http://ward.scripps.edu/gld/) resulting in a total of 302 IGHV, 206 IGKV, and 165 IGLV genes/alleles. This updated database was then converted into a custom IgBLAST database and subsequently used to analyze our BG505-specific mAbs sequences with IgBLAST (Ye et al., 2013).

Antigen-specific mAbs isolated from BG505 SOSIP.664 trimer-immunized RMs

To better understand the immunogenicity of the BG505 SOSIP.664 trimers in previously immunized Indian origin RMs (Sanders et al., 2015) we selected the two animals (rh1987 and rh2011) with the highest serum neutralization activity against the autologous BG505.T332N pseudovirus for in-depth mAb analysis. Peripheral blood mononuclear cells (PBMCs) from the following time points were selected for BG505 SOSIP.664 trimer-specific IgG-positive single memory B-cell sorting: (i) two weeks prior to the fourth immunization (week 22), (ii) 1 week after the fourth immunization (week 25) and (iii) 1 week after the sixth immunization (week 53) (Fig 1A). In total, 25 and 17 mAbs were cloned from RMs rh1987 and rh2011, respectively (Fig 1B).

The BG505-specific mAb sequences were analysed using our germline database and shown to be evenly distributed between kappa and lambda light chains (KC and LC) usage (Fig 1B). For animal rh1987, 11 KC and 14 LC mAbs were isolated. Their average heavy chain (HC) SHM (nucleotide level) was 6.4% (range: 2.1%-10.2%) with an average HC complementarity-determining region 3 (CDR-H3) length of 15 amino acids (aa) (range: 7-23) (Table S2). The rh1987 KC mAbs utilized HC variable genes from the IGHV3 and IGHV4 families and predominantly used KC V genes from the IGKV1 family (Table S2). All of the rh1987 KC mAbs had a CDR-L3 length of 9 aa and their average KC SHM (nucleotide level) was 4.7% (range: 2.6%-6.0%) (Table S2). A single clonal family with 4 members (RM19A) was detected among rh1987 KC mAbs with members isolated from both week 22 and week 25 samples (Table S2). The rh1987 LC mAbs used HC V genes from the IGHV1, IGHV3 and IGHV4 families and LC V genes mainly from the IGLV2 gene family (Table S2). The rh1987 LC mAbs had an average CDR-L3 length of 10 aa (range: 9-11) with an average LC SHM (nucleotide level) of 3.8% (range: 0.9%-10.6%) (Table S2). Two clonal families (RM19B [2 members] and RM19C [4 members]) were identified among the rh1987 LC mAbs isolated from weeks 22 and 25 (Table S2).

For animal rh2011, 8 KC and 9 LC mAbs were isolated. Their average HC SHM rate (nucleotide level) was 6.1% (range: 3.0%-9.1%) and they had an average CDR-H3 length of 17 aa (range 10-20) (Table S2). Half of the rh2011 KC mAbs belonged to the RM20E clonal family, isolated from the week 53 sample. The RM20E clonal family utilized the HC V gene IGHV5-ABI*01_S2502 and the KC V gene LJI.Rh_IGKV2.71 (Table S2). Overall, the rh2011 KC mAbs had an average KC SHM rate (nucleotide level) of 4.1% (range: 3.0%-5.3%) and a CDR-L3 length of 9 aa (Table S2). Among the rh2011 LC mAbs, two clonal families (RM20A [4 members] and RM20B

153 [2 members]) were isolated from weeks 22 and 25 samples (Table S2). Overall, the rh2011 mAbs
154 had an average LC SHM rate (nucleotide level) of 4.4% (range: 2.1%-6.4%) and an average CDR
155 L3 length of 10.6 aa (range: 9-11) (Table S2).
156
157 **BG505-specific mAbs recognize multiple Env regions**
158 All 42 mAbs bound to the BG505 SOSIP.664 trimer in ELISA, but only 11 of the 25 mAbs from
159 rh1987 and 9 of the 17 from rh2011 bound the corresponding gp120 monomer (Fig S1). The mAbs
160 were tested for neutralization activity against the autologous BG505 clade A Tier 2 virus, its
161 glycan-611 knockout variant (N611A), and the heterologous SF162 clade B Tier 1A virus. Only a
162 few mAbs, 4 from rh1987 and 2 from rh2011, neutralized the BG505.T332N pseudovirus but one
163 of them, RM20F from rh2011, did so potently (Fig 1C). Two mAbs from rh1987 and 4 from rh2011
164 were able to potently neutralize the N611A-variant despite lacking activity against the autologous
165 BG505.T332N pseudovirus (Fig 1C and D). None of the 42 mAbs neutralized the easy-to-neutralize
166 heterologous SF162 virus (Fig 1C and D).
167
168 **EM-based epitope mapping revealed mAbs isolated from both animals target 4 distinct, but**
169 **somewhat overlapping epitopes**
170 We used low resolution, negative stain, single particle electron microscopy (EM) to visualize
171 where a representative subset of the isolated mAbs bound on the surface of the BG505 SOSIP
172 trimer. The majority (55%) of mAbs isolated were non-neutralizing antibodies that bound to the
173 base of the BG505 SOSIP trimer (Figs 2A, S2, and Table S2) at a neo-epitope cluster that is
174 occluded by the viral membrane on HIV-1 virions. Fabs bound to the base of the soluble trimer

via multiple angles of approach and utilized a variety of heavy and light chain genes/alleles to do so (Fig 2A and Table S2). The extent of SHM in the base-targeting mAbs ranged from 2-10% in the HC and 1-11% in the light chain (Table S2). Previous studies examining the polyclonal antibody responses elicited by the BG505 SOSIP trimers in rabbits and RMs have shown that epitopes at the base of the soluble trimer were targeted in every single animal analyzed (Bianchi et al., 2018; Cirelli et al., 2019; Nogal et al., 2019). Taken together with our new data, it is clear that the base of SOSIP trimers contain an immunodominant non-neutralizing neo-epitope cluster that is easily targeted by a variety of precursor BCRs in different species.

A subset of mAbs from both animals bound to an epitope near the N611 glycan (Figs 2B and S2). These mAbs were not capable of neutralizing the autologous BG505.T332N pseudovirus but neutralized the BG505 N611A variant (Fig 1C and D). Two additional mAbs isolated from rh2011 (RM20F and RM20H) bound to an epitope near the fusion peptide (FP) and were capable of neutralizing both the autologous and N611A BG505 pseudoviruses, but the latter virus more potently (Figs 2C and S2). MAbs from both animals targeted the 289-glycan hole epitope on BG505, with some, isolated from rh1987, showing weak neutralization of the autologous BG505.T332N pseudovirus (Figs 1C and 2D; Table S2). Multiple germline genes/alleles were used to target the same 289-glycan hole epitope (Table S2).

To further assess the epitopes targeted following immunization with the BG505 SOSIP.664 trimer and verify that we isolated mAbs representative of the full serum antibody response, we performed electron microscopy polyclonal epitope mapping (EMPEM) (Bianchi et al., 2018) using week 28 serum. EMPEM revealed that similar epitopes were targeted in both

196 animals and that the epitope assignments correlated well with the epitopes ascribed to mAbs
197 generated by antigen-specific B-cell sorting (Fig 2E versus S2).

198 A previous analysis of purified serum IgGs from RMs rh1987 and rh2011 identified the
199 C3/V5 epitope as a major target for neutralization activity (Klasse et al., 2018); however, none of
200 the mAbs isolated here targeted the C3/V5 epitope nor were they detected by EMPEM. While
201 low resolution, negative stain EM provides valuable information on where mAbs bind on the
202 surface of HIV-1 Env, the molecular detail necessary to guide structure-based immunogen design
203 requires high-resolution structural data obtained by cryoEM and x-ray crystallography. We
204 therefore selected three Fabs (RM20J, RM20F, and RM20E1) that bound to different epitopes for
205 high-resolution structural determination.

206

207 **MAb RM20J binds to the α2 helix of gp120 and exploits a hole in the glycan shield of BG505 at**
208 **position 289**

209 We solved a 2.3 Å crystal structure of unliganded RM20J Fab and a 3.9 Å cryoEM structure
210 of RM20J Fab bound to the BG505 SOSIP Env trimer (Figs 3A and S3; Tables S4 and S5.). Together
211 these structures revealed the RM20J Fab binds to an epitope on a single gp120 protomer with
212 982 Å² of buried surface area (BSA). The CDR-H1 and CDR-H2 make contact with the C2 region of
213 gp120 including residues N289 and T290 (Fig 3B). A glycan at position N289 would directly clash
214 with both the CDR-H1 and CDR-H2 of RM20J (Fig 3B). CDR-L2 makes contact with the first N-
215 acetyl glucosamine sugar of the N355 glycan (Fig 3C). Additional contacts are made to the α2
216 helix of gp120 by RM20J CDR-H3 and CDR-L2 (Fig 3C). When compared to 10A, a previously
217 characterized 241/289 glycan hole targeting NAb isolated from a BG505 SOSIP.664-immunized

rabbit (Bianchi et al., 2018; McCoy et al., 2016), RM20J binds to an epitope biased more towards 289 and away from 241 in the 241/289 glycan hole, revealing subtle differences in the recognition of the epitope (Figs 3D and 3E). Despite binding to the BG505 SOSIP trimer with high affinity (Table S3), RM20J was not able to neutralize the autologous BG505.T332N pseudovirus (Fig 1C). Although the hypervariable region of V4 was not resolved in the trimer structure, it lies directly above the RM20J epitope and contains two additional glycans (N406 and N411) that may affect RM20J binding. Comparisons between the glycosylation profiles of the BG505 viral Env and the SOSIP.664 trimer revealed differences in the glycoforms present at positions N355, N406, and N411 (Cao et al., 2018; Struwe et al., 2018) with more complex glycans being found on the viral Env that could hinder the ability of RM20J to bind on the surface of the virus and, therefore, render it incapable of neutralization. Several of the mAbs isolated from rh1987, including the RM19A clonal family, bind to a similar epitope as RM20J (Fig 2D, Fig S2, Table S2) and either fail to neutralize the autologous BG505 virus or do so with weak potency (Fig 1C and D).

MAb RM20F binds to a quaternary epitope at the gp120/gp41 interface that includes elements of the fusion peptide and the N88 glycan

For a more detailed view of the mode of RM20F recognition, we solved a 2.2 Å crystal structure of unliganded RM20F Fab and a 4.3 Å cryoEM structure of RM20F Fab bound to BG505 SOSIP trimer (Figs 4A and S3; Tables S4 and S5). RM20F recognizes an epitope spanning two gp41 protomers and a single gp120 protomer that has 1126 Å^2 of BSA at the interface. The RM20F LC contributes 22% of the paratope surface area (250 Å^2) and makes contact with the poorly conserved residues H85 (8.1% prevalence among global strains) and K229 (12.5% prevalence) in

the C1 and C2 regions of gp120 respectively (Fig 4B). The RM20F HC contributes the remaining 78% of the paratope surface area (876 Å²) and uses its 20 residue CDR-H3 to wedge between the FP of the primary gp41 protomer and the HR2 helix of the adjacent gp41 protomer (Fig 4C). Additional contacts with the fusion peptide proximal region (FPPR) of the primary gp41 protomer are made by residues at the tip of CDR-H2 (Fig 4B). The N88 glycan accounts for 18% (198 Å²) of the epitope BSA and makes contact with the CDR-H2 and FR-H3 regions of RM20F (Fig 4B). The lack of connecting density, even at lower contour, between RM20F and the glycans at N611 and N637 suggests these glycans do not substantially contribute to the epitope. Epitope mapping using BG505.T332N mutant pseudoviruses showed that knocking out the N611 glycan (N611Q mutant) substantially enhanced neutralization by RM20F, while knocking out the N637 glycan (N637Q mutant) had no effect. (Fig 4D). Other virus mutants revealed that neutralization by RM20F was sensitive to various sequence changes within the epitope, particularly at residues H85 and E647 (84.3% prevalence) and N88 (N88 glycan knock out) (Fig 4D). The N88 glycan knock out and the H85A mutation (to a lesser extent) significantly reduced neutralization activity of the FP-targeting bNAb VRC34, but no effect on the CD4 binding site targeting bNAb VRC01 (Fig 4D). Introducing the 241 or 289 glycans (S241N and P291T, respectively) modestly reduced the neutralization activity of RM20F (Fig 4D). In comparison to the FP-targeting bNAbs VRC34 and ACS202, RM20F lacked neutralization breadth when tested against a panel that included multiple heterologous viruses (Fig S4) likely due to the dependency on poorly conserved residues.

MAb RM20E1 binds to the fusion peptide and makes contact with two adjacent protomers

We solved a 2.3 Å crystal structure of the unliganded RM20E1 Fab and 4.4 Å cryoEM structure of RM20E1 Fab bound to BG505 SOSIP trimer and Fab PGT122 (Figs 5A and S3; Tables S4 and S5). RM20E1 binds to an epitope composed of one gp120 and two gp41 protomers with 1178 Å² of BSA. Residues 515 to 520 of the FP in the primary gp41 protomer are sandwiched between CDR-H3, CDR-L1, and CDR-L3 of RM20E1 (Fig 5B). CDR-H3 and FR-H1 make contact with HR2 in the adjacent gp41 protomer (Fig 5C). Additionally, the FR-H1 makes contact near the N611-glycan site in the adjacent gp41 protomer, but we observed no connecting density that could be attributed to the N611-glycan itself (Fig 5C). RM20E1 avoids the N88 glycan but does interact with residues in the C1 region of gp120, including H85, via its CDR-L1 (Fig 5B). Despite recognition of the conserved FP, RM20E1 did not neutralize the autologous BG505.T332N pseudovirus. The antibody did however potently neutralize the N611A glycan KO BG505 pseudovirus (Fig 1C) suggesting the epitope is shielded by the N611 glycan. The epitopes of the FP-targeting bNAbs VRC34, ACS202, and DFPH-a.15 overlap to a large extent with the epitopes of RM20E1 and RM20F (Fig 5D), with DFPH-a.15 and VRC34 also neutralizing more potently in the absence of the N611 glycan (Kong et al., 2019; Kong et al., 2016; van Gils et al., 2016; Yuan et al., 2019). The RM20E1-bound FP conformation is similar to the FP conformation when bound by the bNAb VRC34 (Fig S5); however, the inability of RM20E1 to accommodate the N611 glycan likely results in the lack of neutralization of the wild-type virus.

Discussion

A major goal of HIV-1 vaccine research is to elicit bNAbs able to neutralize the large diversity of circulating HIV-1 strains in humans. However, how to achieve this goal remains a

283 critical problem. Native-like Env trimers are an important design platform for engineering
284 immunogens for bNAb induction (de Taeye et al., 2015; Dubrovskaya et al., 2019; Escolano et al.,
285 2019; Escolano et al., 2016; Kong et al., 2019; Sanders et al., 2013; Steichen et al., 2016; Torrents
286 de la Pena et al., 2017; Yang et al., 2018). BG505 SOSIP trimers were able to induce responses in
287 immunized RMs that potently neutralized the autologous Tier 2 virus (Pauthner et al., 2017;
288 Sanders et al., 2015). When present at sufficient titers, those NAbs protected against BG505-SHIV
289 challenge (Pauthner et al., 2019). Evaluating SOSIP trimers in RMs can yield valuable information
290 because of the close genetic relationship between RMs and humans. Here, we isolated mAbs
291 from two BG505 SOSIP.664 trimer-immunized RMs to better understand how the immune
292 system recognizes the trimers and the epitopes associated with the potent, but limited, HIV-1
293 Tier 2 neutralization.

294 By mapping the epitopes of all of the mAbs isolated from the immunized RMs, rather than
295 focusing only on NAbs, we were able to identify several non-neutralizing and potentially
296 immunodominant epitopes that would ideally be eliminated in future immunization studies. As
297 shown previously with mAbs from rabbits immunized with BG505 SOSIP.664 trimers (McCoy et
298 al., 2016), the lack of glycans at positions 241 and 289 in BG505 creates a large glycan hole which
299 is targeted by mAbs from both RMs. The mAbs isolated from RMs that target the 241/289 glycan
300 hole are more biased towards the 289-site compared to the previously characterized rabbit
301 mAbs. This difference may be attributed to the underlying differences in BCR repertoires
302 between the two animal models. In addition to the lack of glycans due to missing sequons that
303 encode for glycosylation, the recombinant BG505 SOSIP.664 trimer may also contain missing
304 glycans even when the correct sequon is present as previously observed by mass spectrometry

studies of glycopeptides (Cao et al., 2017; Cao et al., 2018). Our study identified gp120/gp41 interface antibodies whose neutralization was enhanced in the absence of the N611 glycan, suggesting that the BG505 SOSIP.664 trimer may have sub-stoichiometric glycan occupancy in gp41 at this position, creating an unexpected but immunogenic glycan hole. The elicitation of FP targeting mAbs in RMs with the BG505 SOSIP.664 trimer provides evidence that the FP bNAb epitope is accessible and immunogenic on soluble Env trimer immunogens. Recent studies in mice, guinea pigs and RMs using synthetically produced HIV fusion peptides covalently attached to carrier proteins as priming immunogens followed by boosts with soluble Env trimer immunogens have also elicited FP specific antibodies including some mAbs with neutralization breadth (Cheng et al., 2019; Kong et al., 2019; Xu et al., 2018). However, the majority of the animals immunized in these studies do not develop neutralization breadth and instead develop potent neutralization against the BG505 pseudovirus with the N611 glycan KO (Cheng et al., 2019; Kong et al., 2019; Xu et al., 2018). Given the consistency across studies and animal models in eliciting potent NAbs that target the FP epitope and require the absence of the N611 glycan, investing in strategies to quantify and enhance the N611 glycan occupancy in soluble Env trimer immunogens, particularly for boost immunogens, may improve the neutralization breadth elicited by FP-targeting immunization protocols.

The sorting probe used to isolate BG505 Env-specific B-cells was a C-terminally biotinylated BG505 SOSIP.664 trimer bound to a fluorescent streptavidin tetramer. Steric constraints between the base of the trimer and the streptavidin tetramer likely resulted in a lower recovery of base epitope-specific B-cells. Despite this potential selection bias, 55% of the mAbs isolated from the two immunized RMs bound to the base of the BG505 SOSIP.664 trimer,

indicating the base of the soluble trimer is the major target for antibody responses during immunization. To reduce the immunogenicity of this epitope, glycans can be introduced to shield this site or the native-like trimers could be constructed onto scaffolds or particles (Brouwer et al., 2019; Georgiev et al., 2018; Kulp et al., 2017; Ringe et al., 2019).

We were unable to construct individual germline BCR databases from RMs rh1987 and rh2011 to precisely determine the SHM and gene/alleles usage as samples of naïve PBMC samples were no longer available. Instead, we constructed a germline database containing BCR gene/alleles from multiple Indian origin RMs that allowed us to measure SHM levels in the mAbs we isolated from RMs. The new database provides web-based access (http://ward.scripps.edu/gld/) to a curated and highly annotated general resource for examining BCR gene/alleles from Indian origin RMs. Previous estimates of average SHM rates in mAb sequences from Env-immunized RMs were 8.9% and 6.1% for the HC and LC, respectively (Wang et al., 2017). These apparently high levels of SHM following repeated immunization with the exact same soluble Env immunogens were likely due to missing germline gene/alleles from the database used to calculated SHM. Using the germline database reported in this study, we were able to assign vaccine-elicited antibody sequences to specific germline genes/alleles and determine levels of SHM much more accurately. The average levels of SHM reported in this study (6.3% for HC and 4.2% for LC) are comparable to the average levels of SHM reported in similar immunization studies where per animal germline BCR databases were inferred using IgDiscover (Martinez-Murillo et al., 2017; Phad et al., 2020). Our germline database provides a resource for assigning germline genes/alleles and accurately calculating rates of SHM when inferring individual germline databases for each animal is logistically impractical.

In conclusion, in this study, neutralizing and non-neutralizing mAbs with distinctive epitopes were isolated and characterized in BG505 SOSIP.664-immunized RMs. We demonstrated that a polyclonal response was elicited in two different RMs that target the BG505 SOSIP.664 trimer in highly similar ways. While rabbit antibody responses are dominated by the base and 241-glycan hole epitopes, the RM mAbs target more diverse epitopes with mAbs also targeting the FP and gp120/gp41 interface. The mAbs characterized here also provide a valuable resource for epitope mapping and comparison to a wide array of BG505-based immunization experiments, including the recently initiated BG505 SOSIP.664 human clinical trial (NCT03699241). Finally, the FP-targeting mAbs in particular provide a structure-guided opportunity to modify BG505 SOSIP and other trimers to focus the antibody response on the FP-region, with the goal of eliciting bNAb-like antibodies.

Methods

Immunizations of rhesus macaques

Immunization samples used in this study were obtained from previously immunized RMs described in Sanders et al. 2015 (Sanders et al., 2015). Briefly, RMs were immunized intramuscularly (i.m.) with 100 µg of BG505 SOSIP.664 trimer formulated in 75 units of ISCOMATRIX given at week 0, 4, 12, 24, 38 and 52. All immunizations and blood samplings were performed at the Wisconsin National Primate Research Center as described previously (Sanders et al., 2015).

Rhesus macaque naïve B-cell repertoire sequencing

Frozen PBMCs from five naïve Indian origin RMs were obtained from Yerkes National Primate Research Center (IACUC approval YER2001036). The cells were rapidly thawed in a 37°C water bath and immediately diluted into 10 mL of pre-warmed RPMI media with 10% (v/v) heat-inactivated fetal bovine serum (FBS). Cells were pelleted at 400xg for 7 minutes and resuspended in 0.5 mL FACS buffer (PBS + 1% (v/v) FBS and stained on ice for 1 hr with the panel of fluorescent antibodies against IgM ([clone G20-127] BD), CD4 ([clone OKT-4] BioLegend), CD3 ([clone SP34-2] BD), IgG ([clone G18-145] BD), CD20 ([clone 2H7] BioLegend), CD8 ([clone RPA-T8] BioLegend), CD14 ([clone M5E2] BD), CD16 ([clone eBioCB16] ThermoFisher) and an eFluor780 viability marker (ThermoFisher). A MoFlo Astrios cell sorter (Beckman Coulter), with gating for live $IgM^+/CD20^+/CD3^-/CD4^-/CD8^-/CD14^-/CD16^-$ cells, was used to isolate cells that were then pelleted at 600xg for 10 min, resuspended in RLT+BME buffer (Qiagen), snap frozen in a dry ice ethanol bath and stored at -80°C. RNA extraction was performed using RNeasy Protect Mini kit (Qiagen) following the manufacturer's instructions. The 5' rapid amplification of cDNA ends (5'RACE) with template switching method was used to obtain cDNA with unique molecular identifiers (UMIs) using a protocol modified from Turchaninova *et al.* (Turchaninova et al., 2016). Briefly, 300 ng of RNA was used in a 5'RACE cDNA synthesis reaction. The first-strand cDNA synthesis was performed at 42°C for 1 hr using the RM IgM outer reverse primer (5'-GTGATGGAGTCGGGAAGGAAG-3'), a template switch adaptor with incorporated UMIs (5'-AAGCAGUGGTAUCAACGCAGAGUNNNNUNNNNUNNNNUCTTrGrGrGrG-3'), and SMARTScribe Reverse Transcriptase (Clontech). Residual template switch adaptor was removed by incubation with 5 U of uracil DNA glycosylase (New England BioLabs) for 40 min at 37°C. The resulting cDNA was purified using the MinElute PCR Purification Kit (Qiagen) following the manufacturer's

instructions. PCR amplification was performed using the Q5® High-Fidelity DNA Polymerase (New England BioLabs), the forward primer (5'-NNNNAAGCAGTGGTATCAACGCA-3'), and the RM IgM inner reverse primer (5'-NNNNNAGGGGGAAAAGGGTTG-3'). Illumina adaptors were added using the NEBNext® Ultra™ II DNA Library Prep Kit (New England BioLabs) following the manufacturer's instructions. Libraries were sequenced on an Illumina MiSeq using the Illumina v3, (2x 300 bp) sequencing kit.

Indian origin RM germline BCR database

Gene/alleles published by Vigdorovich *et al*. (Vigdorovich et al., 2016) were aligned to the Mmul_8.0.1 Indian origin RM genome assembly using BLAST (Johnson et al., 2008; Zimin et al., 2014). Sequences that were not identical to the reference genome were eliminated. Additional full-length genes/alleles from available Indian origin RM genomic DNA sequencing datasets (Cirelli et al., 2019; Ramesh et al., 2017) were added to the database. Duplicates and sequences containing ambiguous bases were removed. The resulting initial Indian origin RM germline BCR database (Table S1) was used for running IgDiscover on additional NGS datasets that were obtained during this study as described above, downloaded from the NCBI SRA (Corcoran et al., 2016; Guo et al., 2015), or obtained directly from the study authors (Vigdorovich et al., 2016). Paired sequence reads were aligned and filtered for length and quality using VDJServer (Christley et al., 2018). Novel germline BCR gene/alleles were inferred using IgDiscover v0.11 with the germline_filter parameters "unique_cdr3s" and "unique_js" set to 10 and 4 respectively to reduce the rate of false positives (Corcoran et al., 2016). Inferred genes/alleles were kept if they were detected in more than one animal or if they were identical to RM genes/alleles that were previously deposited in NCBI. The resulting germline BCR database (available at

http://ward.scripps.edu/gld/) was converted into a custom IgBLAST database and subsequently used to analyze the BG505-specific mAb sequences (Ye et al., 2013).

Env sequence analysis

Prevalence of specific amino acids or potential N-linked glycosylation sites (PNGS) were calculated using HIVAnchor (https://github.com/chazbot72/anchor). Pairwise alignments between the HxB2 Env reference sequence (K03455) and the LANL 2018 Group M super filtered web alignment was performed using Clustal Omega (Sievers and Higgins, 2018). The results were parsed into a database keyed on positions relative to the reference, with gaps notated as sub positions following the last identical residue. The database was subsequently interrogated for conservation of amino acids or PNGS at specific positions.

Env protein production

BG505 SOSIP.664, BG505 SOSIP.664-D7324 tag, BG505 SOSIP.664-AviTag, BG505 SOSIP.v4.1, and BG505 SOSIP.v5.2 were expressed in HEK293F cells and purified with either PGT145 or 2G12 affinity chromatograph followed by size exclusion chromatography (SEC) using a HiLoad® 16/600 Superdex® pg200 (GE Healthcare) as described previously (de Taeye et al., 2015; Sanders et al., 2013; Torrents de la Pena et al., 2017). Monomeric gp120 proteins (AviTag or D7324 tagged) were purified using a *Galanthus nivalis* lectin (Vector Labs) column. The Avi-tagged proteins were biotinylated using the BirA enzyme (Avidity) according to the manufacturer's protocol. The resulting biotinylated proteins are referred to using the descriptor AviB.

Monoclonal antibody isolation

BG505 SOSIP.664-specific IgG^+ memory B-cells from isolated PBMCs from RMs rh1987 and rh2011 were single cell sorted in lysis buffer in order to amplify the antigen-specific mAbs, as

previously described (Sok et al., 2014). PBMCs were stained with primary fluorophore-conjugated antibodies to human CD3, CD8, CD14, CD20, IgG and IgM (BD Pharmigen). For staining with Env proteins, 50 nM of BG505 SOSIP.664-AviB, BG505 SOSIP.664 7C3-AviB or gp120-AviB were coupled in equimolar ratios to Streptavidin-PE, Streptavidin-FITC or Streptavidin-APC (Life Technologies), respectively. Cells were stained for 1 hr at 4°C in PBS supplemented with 1 mM EDTA and 1% FBS. In the gating strategy, we first excluded unwanted cell populations ($CD3^-/CD8^-/CD14^-$) followed by selection of HIV Env-specific (positive for any of the 3 probes) memory B-cells ($CD20^+/IgG^+/IgM^-/HIV^+$). Cells of interest were single-cell sorted using a BD FACSAria III machine, into 96-well plates containing lysis buffer, and immediately stored at -80°C. One round of reverse-transcription and two rounds of nested PCR were performed to amplify the antibody V(D)J genes as previously described by Tiller *et al.*[15]. The PCR products containing the variable regions of the heavy chain or light chain, kappa or lambda were cloned into human IgG expression vectors to produce mAbs as described previously (Sok et al., 2014). Fab expression vectors were made by introducing two stop codons following residue D234 (Kabat numbering (Kabat, 1991)) in the IgG heavy chain vectors using the QuikChange® Lightning Site-Directed Mutagenesis kit (Agilent). Sequences were verified by Sanger sequencing (Genewiz).

Monoclonal antibody and Fab production

MAbs and Fabs were expressed in HEK293F cells and purified using affinity chromatography. Briefly, HEK293F cells (Invitrogen) were co-transfected with heavy and light chain plasmids (1:1 ratio) using PEImax. Transfections were performed according to the manufacturer's protocol. Supernatants were harvested 4-6 days following transfection and passed through a 0.45 µm filter. MAbs were purified using Protein A/G (ThermoFisher) or MAbSelect™ (GE Healthcare) affinity

458 chromatography. Fabs were purified using CaptureSelect™ CH1-XL (ThermoFisher) affinity
459 chromatography.

460 **D7324-capture ELISA for monomeric and trimeric BG505 Env proteins**

461 Binding ELISAs were conducted as described previously (Sanders et al., 2013; van Gils et al., 2016).

462 **TZM-bl cell-based neutralization assays**

463 Neutralization assays using the autologous BG505.T332N virus and mutants, and the
464 heterologous SF162 virus, were carried out as described previously (Derking et al., 2015).
465 Nonlinear regression curves were determined and 50% inhibitory concentration (IC_{50}) values
466 were calculated using a sigmoid function in Graphpad Prism v7.03.

467 **Bio-Layer Interferometry (BLI)**

468 An Octet RED instrument (FortéBio) was used to determine the kinetic parameters of the
469 antibody–antigen interactions by Biolayer Interferometry. Monoclonal Fabs were loaded onto
470 anti-human Fab-CH1 (FAB2G) biosensors (FortéBio) at a concentration of 10 µg/mL in kinetics
471 buffer (PBS, pH 7.4, 0.01% [w/v] BSA, and 0.002% [v/v] Tween 20) until a response of 1 nanometer
472 shift was reached. Loaded biosensors were dipped into kinetics buffer for 1 min to acquire a
473 baseline and then moved to wells containing a series of 2-fold dilutions of BG505 SOSIP.v5.2 in
474 kinetics buffer, starting at a 4000 nM. The trimers were allowed to associate for 180 secs before
475 the biosensor were move back to the wells containing kinetics buffer where the baseline was
476 acquired. Disassociation of the trimers from the Fab-loaded biosensors was recorded for 300
477 secs. All BLI experiments were conducted at 37°C. Kinetic parameters were calculated using the
478 Octet System Data Analysis v9.0 (FortéBio).

479 **Negative Stain Electron Microscopy**

BG505 SOSIP/Fab complexes were made by mixing 10-15 µg SOSIP with a 3 to 6-fold per protomer molar excess for monoclonal Fabs or 500 µg polyclonal Fabs and allowed to incubate for 18 to 24 hrs at room temperature (RT). Complex samples were either diluted to 0.02 mg/mL and applied to glow discharged negative stain grids or they were SEC purified using a Superose^{TM} 6 Increase 10/300 GL (GE Healthcare) column to remove excess Fab prior to EM grid preparation. Fractions containing the SOSIP/Fab complexes were pooled and concentrated using 10 kDa Amicon® spin concentrators (Millipore). Samples were diluted to 0.03 mg/mL in TBS (0.05 M Tris pH 7.4, 0.15 M NaCl) and adsorbed onto glow discharged carbon-coated Cu400 EM grids (Electron Microscopy Sciences) and blotted after 10 seconds. The grids were then stained with 3 µL of 2% (w/v) uranyl formate, immediately blotted, and stained again for 45 secs followed by a final blot. Image collection and data processing was performed as described previously on either an FEI Tecnai T12 microscope (2.05 Å/pixel; 52,000× magnification) or FEI Talos microscope (1.98 Å/pixel; 72,000× magnification) with an electron dose of ~25 electrons/Å^2 using Leginon (Pugach et al., 2015; Suloway et al., 2005). 2D classification, 3D sorting and 3D refinement conducted using Relion v3.0 (Zivanov et al., 2018). EM density maps were visualized using UCSF Chimera and segmented using Segger (Pettersen et al., 2004; Pintilie et al., 2010).

X-ray Crystallography Data Collection and Processing

All crystals were grown using sitting drop vapor diffusion. The RM20F Fab was crystallized from a solution containing 10 mg/mL protein in TBS with a well solution containing 0.1M MES, pH 5.0 and 2M ammonium sulfate. The crystals were cryoprotected by soaking in a well solution supplemented with 30% ethylene glycol. The RM20J Fab was crystallized from a solution containing 10 mg/mL protein in TBS with a well solution containing 0.1M MES, pH 6.0, 5%

PEG3000 and 40% PEG400, with no cryoprotectant supplemented. The RM20E1 Fab was crystallized from a solution containing 6.3 mg/mL protein in TBS with a well solution containing 0.1M glycine, pH 10.5, 1.2M NaH_2PO_4, 0.8M Na_2HPO_4, and 0.2M Li_2SO_4, with 15% ethylene glycol supplemented as cryoprotectant. All crystals were grown at 298 K. Diffraction data for RM20F and RM20E1 were collected at the Stanford Synchrotron Radiation Lightsource (SSRL) beamline BL12−2, and that for RM20J collected at the Advanced Photon Source (APS) beamline 23ID-B. Data collection and processing statistics are detailed in Table S5. Data sets were indexed, integrated, and scaled using the HKL-2000 package (Otwinowski and Minor, 1997). The structures were solved by molecular replacement using PHASER (McCoy et al., 2007) with a homology model (SWISS-MODEL; (Arnold et al., 2006; Biasini et al., 2014; Bordoli et al., 2009)) as a search model and further refined using phenix.refine (Adams et al., 2010) combined with manual building cycles in Coot (Emsley et al., 2010).

Cryo Electron Microscopy Sample Preparation

RM20J complex: 500 µg BG505 SOSIP.v5.2 was mixed with 656 µg RM20J Fab and incubated at RT overnight. The complex was SEC purified using a HiLoad® 16/600 Superdex® pg200 (GE Healthcare) column in TBS. Fractions containing the complex were concentrated to 6.1 mg/mL using a 10 kDa Amicon® spin concentrator (Millipore). 3.5 µL of the complex was mixed with 0.57 µL of 0.04 mM lauryl maltose neopentyl glycol (LMNG) and applied to a C-Flat grid (CF-2/1-4C, Protochips, Inc.), which had been plasma-cleaned for 5 seconds using a mixture of N_2/O_2 (Gatan Solarus 950 Plasma system). The grid was blotted and plunged into liquid ethane using a Vitrobot Mark IV (ThermoFisher).

RM20F complex: 500 µg BG505 SOSIP.v4.1 was mixed with approximately 1,000 µg RM20F Fab and incubated at RT overnight. The complex was SEC purified using a Superose™ 6 Increase 10/300 GL (GE Healthcare) column in TBS. Fractions containing the complex were concentrated to 6 mg/mL using a 10 kDa Amicon® spin concentrator (Millipore). 3 µL of the complex was mixed with 1 µL of a n-Dodecyl-β-D-Maltopyranoside (DDM) solution to a final DDM concentration of 0.06 mM and applied to a C-Flat grid (CF-2/2-4C, Protochips, Inc.), which had been plasma-cleaned for 5 seconds using a mixture of N_2/O_2 (Gatan Solarus 950 Plasma system). The grid was blotted and plunged into liquid Ethane using a Vitrobot Mark IV (ThermoFisher).

RM20E1 complex: 355 µg BG505 SOSIP.v5.2 was mixed with 484 µg RM20E1 Fab and 484 µg PGT122 Fab and incubated at RT overnight. The complex was SEC purified using a HiLoad® 16/600 Superdex® pg200 (GE Healthcare) column in TBS. Fractions containing the complex were concentrated to 4 mg/mL using a 10 kDa Amicon® spin concentrator (Millipore). 3 µL of the complex was mixed with 1 µL of a n-Dodecyl-β-D-Maltopyranoside (DDM) solution to a final DDM concentration of 0.06 mM and applied to a grid (Quantifoil R 1.2/1.3, 400), which had been plasma-cleaned for 5 seconds using a mixture of N_2/O_2 (Gatan Solarus 950 Plasma system). The grid was blotted and plunged into liquid Ethane using a Vitrobot Mark IV (ThermoFisher).

Cryo Electron Microscopy Data Collection and Processing

Samples were imaged on either FEI Titan Krios electron microscope (ThermoFisher) operating at 300 keV (RM20F dataset) or a FEI Talos Arctica electron microscope (ThermoFisher) operating at 200 keV (RM20J and RM20E1 datasets). Both microscopes were equipped with Gatan K2 Summit direct electron directors operating in counting mode. Automated data collection was performed using the Leginon software suite (Suloway et al., 2005). Micrograph movie frames were aligned

and dose-weighted using MotionCor2 (Zheng et al., 2017), and CTF models were determined using Gctf (Zhang, 2016). Particle picking, 2D classification, Ab-initio reconstruction, and 3D refinement were conducted using cryoSPARCv2 (Punjani et al., 2017). Data collection and processing parameters are reported in Table S4.

Initial molecular models of the BG505 SOSIP trimer/Fab complexes were built by docking the Env portion of PDB: 5V8M (Lee et al., 2017) into the EM density maps along with the relevant Fab crystal structures (PDB: 4JY5 was used for PGT122 (Julien et al., 2013b)) using UCSF Chimera (Pettersen et al., 2004). The Fab constant regions were removed due to flexibility in the elbow region as commonly found in Fab structures (Bailey et al., 2018), the appropriate stabilizing mutations (v4.1 or v5.2) were introduced into the Env sequence, and N-linked glycans were added using Coot (van Beusekom et al., 2019). The models were iteratively refined into the EM density maps using RosettaRelax and Coot (Casanal et al., 2019; DiMaio et al., 2009; Emsley et al., 2010; Frenz et al., 2018; van Beusekom et al., 2019). Glycan structures were validated using Privateer (Agirre et al., 2015). Overall structures were evaluated using EMRinger (Barad et al., 2015) and MolProbity (Williams et al., 2018). Protein interface calculations were performed using jsPISA (Krissinel, 2015). Final model statistics are summarized in Table S4.

Statistical analysis

Statistical models inherent to Relion 3.0 (Zivanov et al., 2018) and cryoSPARC (Punjani et al., 2017) were employed in image analysis to derive 2D classes and 3D models. All ELISA and neutralization assays were conducted with at least duplicate measurements.

Data and Software Availability

566 The accession numbers for Env-specific BCR sequences are DDBJ/ENA/GenBank: MT002976-
567 MT002992 and MT008262-MT008328. RM IgM BCR sequences are available under BioProject ID:
568 PRJNA604386. Atomic coordinates and structure factors of the reported crystal structure have
569 been deposited in the Protein Data Bank (PDB: 6VOS, 6VOR). Cryo-EM reconstructions have been
570 deposited in the Electron Microscopy Data Bank (EMDB: EMD-21246, EMD-21257, EMD-21232),
571 and in the Protein Data Bank (PDB: 6VN0, 6VO1, 6VLR). The accession numbers for the negative
572 stain 3D EM reconstructions are Electron Microscopy DataBank: EMD-21053, EMD-21055, EMD-
573 21056, EMD-21057, EMD-21058, EMD-21059, EMD-21061, EMD-21062, EMD-21064, EMD-
574 21065, EMD-21066, EMD-21075, EMD-21076, EMD-21077, EMD-21078, EMD-21079, EMD-
575 21080, EMD-21081, EMD-21082, EMD-21083, EMD-21084, EMD-21085, EMD-21086, EMD-
576 21087, EMD-21088, EMD-21089, EMD-21090, EMD-21091, EMD-21092, EMD-21093, EMD-
577 21272, EMD-21273, EMD-21274, EMD-21275, EMD-21276, EMD-21277, EMD-21278.
578
579 **Figure Legends**
580 **Figure 1.** MAb isolation and characterization from BG505 SOSIP.664 trimer-immunized RMs. (A)
581 Simplified immunization scheme adapted from Sanders et al. 2015 (Sanders et al., 2015). Black
582 arrows indicate i.m. immunizations with 100 μg of BG505 SOSIP.664 with 75 units of ISCOMATRIX
583 adjuvant. Red arrows indicate blood draws. (B) Heavy and light chain genetic characteristics for
584 mAbs isolated from rh1987 and rh2011. (C) TZM-bl neutralization of BG505.T332N,
585 BG505.T332N.N611A, and SF162 pseudoviruses for mAbs isolated from RM rh1987. (D) TZM-bl
586 neutralization of BG505.T332N, BG505.T332N.N611A, and SF162 pseudoviruses for mAbs
587 isolated from RM rh2011. Assay limit of detection was at an IC_{50} of 50 μg/mL.

588 **Figure 2.** Epitope mapping by negative stain electron microscopy. (A) Representative base-
589 targeting mAbs for animals rh1987 and rh2011. (B) Overlapping gp120/gp41 interface epitope
590 targeted by mAbs from both animals. (C) Overlapping FP epitope targeted by mAbs from both
591 animals. (D) Overlapping N289-glycan hole epitope targeted by mAbs from both animals. (E)
592 EMPEM analysis for wk28 IgG from rh2011 and rh1987. All structural figures were generated with
593 UCSF Chimera (Pettersen et al., 2004). EM density maps were segmented with the Segger
594 extension in UCSF Chimera (Pettersen et al., 2004; Pintilie et al., 2010).

595 **Figure 3.** RM20J binds to the N289 glycan hole region of BG505 SOSIP.v5.2 (A) Segmented 3.9 Å
596 cryoEM reconstruction of RM20J Fab (pink) in complex with BG505 SOSIP.v5.2 (gp120, dark blue;
597 gp41, light blue). (B) and (C) Zoomed-in views of the epitope/paratope interaction between
598 gp120 (blue, ribbon diagram) and RM20J Fab (surface representation). (D) and (E) Comparison of
599 the RM20J epitope with that of the BG505 SOSIP.664 elicited rabbit neutralizing NAb 10A (PDB:
600 6DID) (Bianchi et al., 2018; McCoy et al., 2016).

601 **Figure 4.** RM20F binds to a quaternary epitope at the gp120/gp41 interface of BG505 SOSIP.v4.1.
602 (A) Segmented 4.3 Å cryoEM reconstruction of RM20F Fab (orange) in complex with BG505 SOSIP
603 (gp120, dark blue; gp41, light blue). (B) and (C) Zoomed-in views of the epitope/paratope
604 interaction between BG505 SOSIP (gp120, dark blue; gp41s, light blue and light green; ribbon
605 diagram) and RM20F Fab (surface representation). (D) Neutralization data for BG505 mutant
606 pseudoviruses against VRC01, RM20F, and VRC34.

607 **Figure 5.** RM20E1 binds to the fusion peptide of BG505 SOSIP.v5.2. (A) Segmented 4.2 Å cryoEM
608 reconstruction of RM20E1 Fab (yellow) and PGT122 Fab (light green) in complex with BG505
609 SOSIP (gp120, dark blue; gp41, light blue). (B) and (C) Zoomed-in views of the epitope/paratope

610 interaction between BG505 SOSIP (gp120, dark blue; gp41s, light blue and light green; ribbon
611 diagram) and RM20E1 Fab (surface representation). (D) Comparison of RM20E1 and RM20F
612 epitopes to those of FP targeting bNAbs VRC34, ACS202, and DFPH-a.15 (Kong et al., 2019; Kong
613 et al., 2016; van Gils et al., 2016; Yuan et al., 2019).

614 **Table S1.** Initial germline BCR database used in IgDiscover

615

616 **Acknowledgements**

617 We thank Jean-Christophe Ducom, Hannah Turner, and Bill Anderson for assistance with
618 computational resources, microscope management, and data collection. We thank Alan Saluk,
619 Brian Seegers, Steven Head, Jessica Ledesma, Curt Wittenberg, and Nitya Bhaskaran for
620 assistance with naïve B-cell sorting and NGS sequencing. This work was supported by the HIV
621 Vaccine Research and Design (HIVRAD) program (P01 AI110657) (A.B.W., R.W.S, J.P.M., and
622 I.A.W.), NIH CHAVI-ID (UM1 AI100663) and CHAVD (UM1 AI44462) awards (A.B.W., I.A.W. and
623 D.R.B.), NIH R01 AI13082 (J.P.M.), the International AIDS Vaccine Initiative Neutralizing Antibody
624 Center, the Bill and Melinda Gates Foundation CAVD (OPP1115782, OPP1132237, OPP1084519,
625 OPP119635), and the European Union's Horizon 2020 research and innovation program under
626 grant agreement no. 681137 (R.W.S.). C.A.C. is supported by the NIH F31 Ruth L. Kirschstein
627 Predoctoral Award Al131873 and by the Achievement Rewards for College Scientists Foundation.
628 R.W.S. is a recipient of a Vici fellowship from the Netherlands Organization for Scientific Research
629 (NWO). G.O. and M.J.v.G. are supported by amfAR Mathilde Krim Fellowships in Basic Biomedical
630 Research grant numbers 109718-63-RKNT and 109514-61-RKVA, respectively. J.v.S. is a recipient
631 of a 2017 AMC Ph.D. Scholarship. Computational analyses of EM data were performed using

shared instrumentation funded by NIH grant S10OD021634. Naïve B-cell sorting and NGS sequencing was conducted as part of the Technologies Across Scale graduate course with support from Skaggs Graduate School of Chemical and Biological Sciences at Scripps Research. Use of the Stanford Synchrotron Radiation Lightsource, SLAC National Accelerator Laboratory, is supported by the U.S. Department of Energy, Office of Science, Office of Basic Energy Sciences under Contract No. DE-AC02-76SF00515. The SSRL Structural Molecular Biology Program is supported by the DOE Office of Biological and Environmental Research, and by the National Institutes of Health, National Institute of General Medical Sciences (including P41GM103393). The contents of this publication are solely the responsibility of the authors and do not necessarily represent the official views of NIGMS, NIAID, or NIH.

References

Adams, P.D., Afonine, P.V., Bunkoczi, G., Chen, V.B., Davis, I.W., Echols, N., Headd, J.J., Hung, L.W., Kapral, G.J., Grosse-Kunstleve, R.W.*, et al.* (2010). PHENIX: a comprehensive Python-based system for macromolecular structure solution. Acta crystallographica Section D, Biological crystallography *66*, 213-221.

Agirre, J., Iglesias-Fernandez, J., Rovira, C., Davies, G.J., Wilson, K.S., and Cowtan, K.D. (2015). Privateer: software for the conformational validation of carbohydrate structures. Nature structural & molecular biology *22*, 833-834.

Arnold, K., Bordoli, L., Kopp, J., and Schwede, T. (2006). The SWISS-MODEL workspace: a web-based environment for protein structure homology modelling. Bioinformatics *22*, 195-201.

Bailey, L.J., Sheehy, K.M., Dominik, P.K., Liang, W.G., Rui, H., Clark, M., Jaskolowski, M., Kim, Y., Deneka, D., Tang, W.J.*, et al.* (2018). Locking the Elbow: Improved Antibody Fab Fragments as Chaperones for Structure Determination. Journal of molecular biology *430*, 337-347.

Barad, B.A., Echols, N., Wang, R.Y., Cheng, Y., DiMaio, F., Adams, P.D., and Fraser, J.S. (2015). EMRinger: side chain-directed model and map validation for 3D cryo-electron microscopy. Nature methods *12*, 943-946.

Bianchi, M., Turner, H.L., Nogal, B., Cottrell, C.A., Oyen, D., Pauthner, M., Bastidas, R., Nedellec, R., McCoy, L.E., Wilson, I.A.*, et al.* (2018). Electron-Microscopy-Based Epitope Mapping Defines Specificities of Polyclonal Antibodies Elicited during HIV-1 BG505 Envelope Trimer Immunization. Immunity *49*, 288-300 e288.

663 Biasini, M., Bienert, S., Waterhouse, A., Arnold, K., Studer, G., Schmidt, T., Kiefer, F., Gallo
664 Cassarino, T., Bertoni, M., Bordoli, L.*, et al.* (2014). SWISS-MODEL: modelling protein tertiary
665 and quaternary structure using evolutionary information. Nucleic Acids Res *42*, W252-258.
666 Bordoli, L., Kiefer, F., Arnold, K., Benkert, P., Battey, J., and Schwede, T. (2009). Protein
667 structure homology modeling using SWISS-MODEL workspace. Nature protocols *4*, 1-13.
668 Brouwer, P.J.M., Antanasijevic, A., Berndsen, Z., Yasmeen, A., Fiala, B., Bijl, T.P.L., Bontjer, I.,
669 Bale, J.B., Sheffler, W., Allen, J.D.*, et al.* (2019). Enhancing and shaping the immunogenicity of
670 native-like HIV-1 envelope trimers with a two-component protein nanoparticle. Nat Commun
671 *10*, 4272.
672 Burton, D.R., and Hangartner, L. (2016). Broadly Neutralizing Antibodies to HIV and Their Role in
673 Vaccine Design. Annual review of immunology *34*, 635-659.
674 Cao, L., Diedrich, J.K., Kulp, D.W., Pauthner, M., He, L., Park, S.R., Sok, D., Su, C.Y., Delahunty,
675 C.M., Menis, S.*, et al.* (2017). Global site-specific N-glycosylation analysis of HIV envelope
676 glycoprotein. Nat Commun *8*, 14954.
677 Cao, L., Pauthner, M., Andrabi, R., Rantalainen, K., Berndsen, Z., Diedrich, J.K., Menis, S., Sok, D.,
678 Bastidas, R., Park, S.R.*, et al.* (2018). Differential processing of HIV envelope glycans on the virus
679 and soluble recombinant trimer. Nat Commun *9*, 3693.
680 Casanal, A., Lohkamp, B., and Emsley, P. (2019). Current Developments in Coot for
681 Macromolecular Model Building of Electron Cryo-microscopy and Crystallographic Data. Protein
682 science : a publication of the Protein Society.
683 Cheng, C., Xu, K., Kong, R., Chuang, G.Y., Corrigan, A.R., Geng, H., Hill, K.R., Jafari, A.J., O'Dell, S.,
684 Ou, L.*, et al.* (2019). Consistent elicitation of cross-clade HIV-neutralizing responses achieved in
685 guinea pigs after fusion peptide priming by repetitive envelope trimer boosting. PloS one *14*,
686 e0215163.
687 Christley, S., Scarborough, W., Salinas, E., Rounds, W.H., Toby, I.T., Fonner, J.M., Levin, M.K.,
688 Kim, M., Mock, S.A., Jordan, C.*, et al.* (2018). VDJServer: A Cloud-Based Analysis Portal and Data
689 Commons for Immune Repertoire Sequences and Rearrangements. Frontiers in immunology *9*,
690 976.
691 Cirelli, K.M., Carnathan, D.G., Nogal, B., Martin, J.T., Rodriguez, O.L., Upadhyay, A.A., Enemuo,
692 C.A., Gebru, E.H., Choe, Y., Viviano, F.*, et al.* (2019). Slow Delivery Immunization Enhances HIV
693 Neutralizing Antibody and Germinal Center Responses via Modulation of Immunodominance.
694 Cell.
695 Corcoran, M.M., Phad, G.E., Nestor, V.B., Stahl-Hennig, C., Sumida, N., Persson, M.A., Martin,
696 M., and Karlsson Hedestam, G.B. (2016). Production of individualized V gene databases reveals
697 high levels of immunoglobulin genetic diversity. Nat Commun *7*, 13642.
698 de Taeye, S.W., Ozorowski, G., Torrents de la Pena, A., Guttman, M., Julien, J.P., van den
699 Kerkhof, T.L., Burger, J.A., Pritchard, L.K., Pugach, P., Yasmeen, A.*, et al.* (2015). Immunogenicity
700 of Stabilized HIV-1 Envelope Trimers with Reduced Exposure of Non-neutralizing Epitopes. Cell
701 *163*, 1702-1715.
702 Derking, R., Ozorowski, G., Sliepen, K., Yasmeen, A., Cupo, A., Torres, J.L., Julien, J.P., Lee, J.H.,
703 van Montfort, T., de Taeye, S.W.*, et al.* (2015). Comprehensive antigenic map of a cleaved
704 soluble HIV-1 envelope trimer. PLoS pathogens *11*, e1004767.

DiMaio, F., Tyka, M.D., Baker, M.L., Chiu, W., and Baker, D. (2009). Refinement of protein structures into low-resolution density maps using rosetta. Journal of molecular biology *392*, 181-190.

Dubrovskaya, V., Tran, K., Ozorowski, G., Guenaga, J., Wilson, R., Bale, S., Cottrell, C.A., Turner, H.L., Seabright, G., O'Dell, S.*, et al.* (2019). Vaccination with Glycan-Modified HIV NFL Envelope Trimer-Liposomes Elicits Broadly Neutralizing Antibodies to Multiple Sites of Vulnerability. Immunity *51*, 915-929 e917.

Emsley, P., Lohkamp, B., Scott, W.G., and Cowtan, K. (2010). Features and development of Coot. Acta crystallographica Section D, Biological crystallography *66*, 486-501.

Escolano, A., Gristick, H.B., Abernathy, M.E., Merkenschlager, J., Gautam, R., Oliveira, T.Y., Pai, J., West, A.P., Jr., Barnes, C.O., Cohen, A.A.*, et al.* (2019). Immunization expands B cells specific to HIV-1 V3 glycan in mice and macaques. Nature *570*, 468-473.

Escolano, A., Steichen, J.M., Dosenovic, P., Kulp, D.W., Golijanin, J., Sok, D., Freund, N.T., Gitlin, A.D., Oliveira, T., Araki, T.*, et al.* (2016). Sequential Immunization Elicits Broadly Neutralizing Anti-HIV-1 Antibodies in Ig Knockin Mice. Cell *166*, 1445-1458 e1412.

Frenz, B., Ramisch, S., Borst, A.J., Walls, A.C., Adolf-Bryfogle, J., Schief, W.R., Veesler, D., and DiMaio, F. (2018). Automatically Fixing Errors in Glycoprotein Structures with Rosetta. Structure.

Gadala-Maria, D., Yaari, G., Uduman, M., and Kleinstein, S.H. (2015). Automated analysis of high-throughput B-cell sequencing data reveals a high frequency of novel immunoglobulin V gene segment alleles. Proceedings of the National Academy of Sciences of the United States of America *112*, E862-870.

Georgiev, I.S., Joyce, M.G., Chen, R.E., Leung, K., McKee, K., Druz, A., Van Galen, J.G., Kanekiyo, M., Tsybovsky, Y., Yang, E.S.*, et al.* (2018). Two-Component Ferritin Nanoparticles for Multimerization of Diverse Trimeric Antigens. ACS Infect Dis *4*, 788-796.

Guo, K., Halemano, K., Schmitt, K., Katuwal, M., Wang, Y., Harper, M.S., Heilman, K.J., Kuwata, T., Stephens, E.B., and Santiago, M.L. (2015). Immunoglobulin VH gene diversity and somatic hypermutation during SIV infection of rhesus macaques. Immunogenetics *67*, 355-370.

Jardine, J.G., Kulp, D.W., Havenar-Daughton, C., Sarkar, A., Briney, B., Sok, D., Sesterhenn, F., Ereno-Orbea, J., Kalyuzhniy, O., Deresa, I.*, et al.* (2016). HIV-1 broadly neutralizing antibody precursor B cells revealed by germline-targeting immunogen. Science *351*, 1458-1463.

Johnson, M., Zaretskaya, I., Raytselis, Y., Merezhuk, Y., McGinnis, S., and Madden, T.L. (2008). NCBI BLAST: a better web interface. Nucleic Acids Res *36*, W5-9.

Julien, J.P., Cupo, A., Sok, D., Stanfield, R.L., Lyumkis, D., Deller, M.C., Klasse, P.J., Burton, D.R., Sanders, R.W., Moore, J.P.*, et al.* (2013a). Crystal structure of a soluble cleaved HIV-1 envelope trimer. Science *342*, 1477-1483.

Julien, J.P., Sok, D., Khayat, R., Lee, J.H., Doores, K.J., Walker, L.M., Ramos, A., Diwanji, D.C., Pejchal, R., Cupo, A.*, et al.* (2013b). Broadly neutralizing antibody PGT121 allosterically modulates CD4 binding via recognition of the HIV-1 gp120 V3 base and multiple surrounding glycans. PLoS pathogens *9*, e1003342.

Kabat, E.A. (1991). Sequences of proteins of immunological interest : tabulation and analysis of amino acid and nucleic acid sequences of precursors, V-regions, C-regions, J-chain, T-cell receptors for antigenm T-cell surface antigens, [beta]2-microglobulins,major histocompatibility antigens, Thy-1, complement, C-reactive protein, thymopoietin, integrins, post-gamme globulin,

749 [alpha]2-macroglobulins, and other related proteins, 5th edn (Bethesda, Md. (Bethesda,
750 20892): U.S. Dept. of Health and Human Services, Public Health Service, National Institutes of
751 Health).
752 Klasse, P.J., Ketas, T.J., Cottrell, C.A., Ozorowski, G., Debnath, G., Camara, D., Francomano, E.,
753 Pugach, P., Ringe, R.P., LaBranche, C.C.*, et al.* (2018). Epitopes for neutralizing antibodies
754 induced by HIV-1 envelope glycoprotein BG505 SOSIP trimers in rabbits and macaques. PLoS
755 pathogens *14*, e1006913.
756 Kong, R., Duan, H., Sheng, Z., Xu, K., Acharya, P., Chen, X., Cheng, C., Dingens, A.S., Gorman, J.,
757 Sastry, M.*, et al.* (2019). Antibody Lineages with Vaccine-Induced Antigen-Binding Hotspots
758 Develop Broad HIV Neutralization. Cell *178*, 567-584 e519.
759 Kong, R., Xu, K., Zhou, T., Acharya, P., Lemmin, T., Liu, K., Ozorowski, G., Soto, C., Taft, J.D.,
760 Bailer, R.T.*, et al.* (2016). Fusion peptide of HIV-1 as a site of vulnerability to neutralizing
761 antibody. Science *352*, 828-833.
762 Krissinel, E. (2015). Stock-based detection of protein oligomeric states in jsPISA. Nucleic Acids
763 Res *43*, W314-319.
764 Kulp, D.W., Steichen, J.M., Pauthner, M., Hu, X., Schiffner, T., Liguori, A., Cottrell, C.A., Havenar-
765 Daughton, C., Ozorowski, G., Georgeson, E.*, et al.* (2017). Structure-based design of native-like
766 HIV-1 envelope trimers to silence non-neutralizing epitopes and eliminate CD4 binding. Nat
767 Commun *8*, 1655.
768 Landais, E., and Moore, P.L. (2018). Development of broadly neutralizing antibodies in HIV-1
769 infected elite neutralizers. Retrovirology *15*, 61.
770 Lee, J.H., Andrabi, R., Su, C.Y., Yasmeen, A., Julien, J.P., Kong, L., Wu, N.C., McBride, R., Sok, D.,
771 Pauthner, M.*, et al.* (2017). A Broadly Neutralizing Antibody Targets the Dynamic HIV Envelope
772 Trimer Apex via a Long, Rigidified, and Anionic beta-Hairpin Structure. Immunity *46*, 690-702.
773 Lei, L., Yang, Y.R., Tran, K., Wang, Y., Chiang, C.I., Ozorowski, G., Xiao, Y., Ward, A.B., Wyatt, R.T.,
774 and Li, Y. (2019). The HIV-1 Envelope Glycoprotein C3/V4 Region Defines a Prevalent
775 Neutralization Epitope following Immunization. Cell Rep *27*, 586-598 e586.
776 Lyumkis, D., Julien, J.P., de Val, N., Cupo, A., Potter, C.S., Klasse, P.J., Burton, D.R., Sanders,
777 R.W., Moore, J.P., Carragher, B.*, et al.* (2013). Cryo-EM structure of a fully glycosylated soluble
778 cleaved HIV-1 envelope trimer. Science *342*, 1484-1490.
779 Martinez-Murillo, P., Tran, K., Guenaga, J., Lindgren, G., Adori, M., Feng, Y., Phad, G.E., Vazquez
780 Bernat, N., Bale, S., Ingale, J.*, et al.* (2017). Particulate Array of Well-Ordered HIV Clade C Env
781 Trimers Elicits Neutralizing Antibodies that Display a Unique V2 Cap Approach. Immunity *46*,
782 804-817 e807.
783 McCoy, A.J., Grosse-Kunstleve, R.W., Adams, P.D., Winn, M.D., Storoni, L.C., and Read, R.J.
784 (2007). Phaser crystallographic software. J Appl Crystallogr *40*, 658-674.
785 McCoy, L.E., van Gils, M.J., Ozorowski, G., Messmer, T., Briney, B., Voss, J.E., Kulp, D.W.,
786 Macauley, M.S., Sok, D., Pauthner, M.*, et al.* (2016). Holes in the Glycan Shield of the Native HIV
787 Envelope Are a Target of Trimer-Elicited Neutralizing Antibodies. Cell Rep *16*, 2327-2338.
788 Moldt, B., Le, K.M., Carnathan, D.G., Whitney, J.B., Schultz, N., Lewis, M.G., Borducchi, E.N.,
789 Smith, K.M., Mackel, J.J., Sweat, S.L.*, et al.* (2016). Neutralizing antibody affords comparable
790 protection against vaginal and rectal simian/human immunodeficiency virus challenge in
791 macaques. Aids *30*, 1543-1551.

Nogal, B., Bianchi, M., Cottrell, C.A., Kirchdoerfer, R.N., Sewall, L.M., Turner, H.L., Zhao, F., Sok, D., Burton, D.R., Hangartner, L.*, et al.* (2019). Mapping polyclonal antibody responses in non-human primates vaccinated with HIV Env trimer subunit vaccines. bioRxiv, 833715.

Otwinowski, Z., and Minor, W. (1997). Processing of X-ray diffraction data collected in oscillation mode. Methods Enzymol *276*, 307-326.

Pancera, M., Zhou, T., Druz, A., Georgiev, I.S., Soto, C., Gorman, J., Huang, J., Acharya, P., Chuang, G.Y., Ofek, G.*, et al.* (2014). Structure and immune recognition of trimeric pre-fusion HIV-1 Env. Nature *514*, 455-461.

Pauthner, M., Havenar-Daughton, C., Sok, D., Nkolola, J.P., Bastidas, R., Boopathy, A.V., Carnathan, D.G., Chandrashekar, A., Cirelli, K.M., Cottrell, C.A.*, et al.* (2017). Elicitation of Robust Tier 2 Neutralizing Antibody Responses in Nonhuman Primates by HIV Envelope Trimer Immunization Using Optimized Approaches. Immunity *46*, 1073-1088 e1076.

Pauthner, M.G., Nkolola, J.P., Havenar-Daughton, C., Murrell, B., Reiss, S.M., Bastidas, R., Prevost, J., Nedellec, R., von Bredow, B., Abbink, P.*, et al.* (2019). Vaccine-Induced Protection from Homologous Tier 2 SHIV Challenge in Nonhuman Primates Depends on Serum-Neutralizing Antibody Titers. Immunity *50*, 241-252 e246.

Pegu, A., Borate, B., Huang, Y.D., Pauthner, M.G., Hessell, A.J., Julg, B., Doria-Rose, N.A., Schmidt, S.D., Carpp, L.N., Cully, M.D.*, et al.* (2019). A Meta-analysis of Passive Immunization Studies Shows that Serum-Neutralizing Antibody Titer Associates with Protection against SHIV Challenge. Cell Host & Microbe *26*, 336-+.

Pettersen, E.F., Goddard, T.D., Huang, C.C., Couch, G.S., Greenblatt, D.M., Meng, E.C., and Ferrin, T.E. (2004). UCSF Chimera--a visualization system for exploratory research and analysis. J Comput Chem *25*, 1605-1612.

Phad, G.E., Pushparaj, P., Tran, K., Dubrovskaya, V., Adori, M., Martinez-Murillo, P., Vazquez Bernat, N., Singh, S., Dionne, G., O'Dell, S.*, et al.* (2020). Extensive dissemination and intraclonal maturation of HIV Env vaccine-induced B cell responses. The Journal of experimental medicine *217*.

Pintilie, G.D., Zhang, J., Goddard, T.D., Chiu, W., and Gossard, D.C. (2010). Quantitative analysis of cryo-EM density map segmentation by watershed and scale-space filtering, and fitting of structures by alignment to regions. Journal of structural biology *170*, 427-438.

Pugach, P., Ozorowski, G., Cupo, A., Ringe, R., Yasmeen, A., de Val, N., Derking, R., Kim, H.J., Korzun, J., Golabek, M.*, et al.* (2015). A native-like SOSIP.664 trimer based on an HIV-1 subtype B env gene. J Virol *89*, 3380-3395.

Punjani, A., Rubinstein, J.L., Fleet, D.J., and Brubaker, M.A. (2017). cryoSPARC: algorithms for rapid unsupervised cryo-EM structure determination. Nature methods *14*, 290-296.

Ralph, D.K., and Matsen, F.A.I. (2018). Per-sample immunoglobulin germline inference from B cell receptor deep sequencing data. arXiv.

Ramesh, A., Darko, S., Hua, A., Overman, G., Ransier, A., Francica, J.R., Trama, A., Tomaras, G.D., Haynes, B.F., Douek, D.C.*, et al.* (2017). Structure and Diversity of the Rhesus Macaque Immunoglobulin Loci through Multiple De Novo Genome Assemblies. Frontiers in immunology *8*, 1407.

Ringe, R.P., Cruz Portillo, V.M., Dosenovic, P., Ketas, T.J., Ozorowski, G., Nogal, B., Perez, L., LaBranche, C.C., Lim, J., Francomano, E.*, et al.* (2019). Neutralizing antibody induction by HIV-1

Envelope glycoprotein SOSIP trimers on iron oxide nanoparticles may be impaired by mannose binding lectin. J Virol.

Sanders, R.W., Derking, R., Cupo, A., Julien, J.P., Yasmeen, A., de Val, N., Kim, H.J., Blattner, C., de la Pena, A.T., Korzun, J., *et al.* (2013). A next-generation cleaved, soluble HIV-1 Env trimer, BG505 SOSIP.664 gp140, expresses multiple epitopes for broadly neutralizing but not non-neutralizing antibodies. PLoS pathogens *9*, e1003618.

Sanders, R.W., van Gils, M.J., Derking, R., Sok, D., Ketas, T.J., Burger, J.A., Ozorowski, G., Cupo, A., Simonich, C., Goo, L., *et al.* (2015). HIV-1 VACCINES. HIV-1 neutralizing antibodies induced by native-like envelope trimers. Science *349*, aac4223.

Sievers, F., and Higgins, D.G. (2018). Clustal Omega for making accurate alignments of many protein sequences. Protein science : a publication of the Protein Society *27*, 135-145.

Sok, D., van Gils, M.J., Pauthner, M., Julien, J.P., Saye-Francisco, K.L., Hsueh, J., Briney, B., Lee, J.H., Le, K.M., Lee, P.S., *et al.* (2014). Recombinant HIV envelope trimer selects for quaternary-dependent antibodies targeting the trimer apex. Proceedings of the National Academy of Sciences of the United States of America *111*, 17624-17629.

Steichen, J.M., Kulp, D.W., Tokatlian, T., Escolano, A., Dosenovic, P., Stanfield, R.L., McCoy, L.E., Ozorowski, G., Hu, X., Kalyuzhniy, O., *et al.* (2016). HIV Vaccine Design to Target Germline Precursors of Glycan-Dependent Broadly Neutralizing Antibodies. Immunity *45*, 483-496.

Struwe, W.B., Chertova, E., Allen, J.D., Seabright, G.E., Watanabe, Y., Harvey, D.J., Medina-Ramirez, M., Roser, J.D., Smith, R., Westcott, D., *et al.* (2018). Site-Specific Glycosylation of Virion-Derived HIV-1 Env Is Mimicked by a Soluble Trimeric Immunogen. Cell Rep *24*, 1958-1966 e1955.

Suloway, C., Pulokas, J., Fellmann, D., Cheng, A., Guerra, F., Quispe, J., Stagg, S., Potter, C.S., and Carragher, B. (2005). Automated molecular microscopy: the new Leginon system. Journal of structural biology *151*, 41-60.

Torrents de la Pena, A., Julien, J.P., de Taeye, S.W., Garces, F., Guttman, M., Ozorowski, G., Pritchard, L.K., Behrens, A.J., Go, E.P., Burger, J.A., *et al.* (2017). Improving the Immunogenicity of Native-like HIV-1 Envelope Trimers by Hyperstabilization. Cell Rep *20*, 1805-1817.

Turchaninova, M.A., Davydov, A., Britanova, O.V., Shugay, M., Bikos, V., Egorov, E.S., Kirgizova, V.I., Merzlyak, E.M., Staroverov, D.B., Bolotin, D.A., *et al.* (2016). High-quality full-length immunoglobulin profiling with unique molecular barcoding. Nature protocols *11*, 1599-1616.

UNAIDS (2019). Global HIV & AIDS statistics — 2018 fact sheet.

van Beusekom, B., Wezel, N., Hekkelman, M.L., Perrakis, A., Emsley, P., and Joosten, R.P. (2019). Building and rebuilding N-glycans in protein structure models. Acta Crystallogr D Struct Biol *75*, 416-425.

van Gils, M.J., van den Kerkhof, T.L., Ozorowski, G., Cottrell, C.A., Sok, D., Pauthner, M., Pallesen, J., de Val, N., Yasmeen, A., de Taeye, S.W., *et al.* (2016). An HIV-1 antibody from an elite neutralizer implicates the fusion peptide as a site of vulnerability. Nat Microbiol *2*, 16199.

Vigdorovich, V., Oliver, B.G., Carbonetti, S., Dambrauskas, N., Lange, M.D., Yacoob, C., Leahy, W., Callahan, J., Stamatatos, L., and Sather, D.N. (2016). Repertoire comparison of the B-cell receptor-encoding loci in humans and rhesus macaques by next-generation sequencing. Clin Transl Immunology *5*, e93.

Wang, Y., O'Dell, S., Turner, H.L., Chiang, C.I., Lei, L., Guenaga, J., Wilson, R., Martinez-Murillo, P., Doria-Rose, N., Ward, A.B.*, et al.* (2017). HIV-1 Cross-Reactive Primary Virus Neutralizing Antibody Response Elicited by Immunization in Nonhuman Primates. J Virol *91*.

Williams, C.J., Headd, J.J., Moriarty, N.W., Prisant, M.G., Videau, L.L., Deis, L.N., Verma, V., Keedy, D.A., Hintze, B.J., Chen, V.B.*, et al.* (2018). MolProbity: More and better reference data for improved all-atom structure validation. Protein science : a publication of the Protein Society *27*, 293-315.

Wu, X. (2018). HIV Broadly Neutralizing Antibodies: VRC01 and Beyond. Adv Exp Med Biol *1075*, 53-72.

Xu, K., Acharya, P., Kong, R., Cheng, C., Chuang, G.Y., Liu, K., Louder, M.K., O'Dell, S., Rawi, R., Sastry, M.*, et al.* (2018). Epitope-based vaccine design yields fusion peptide-directed antibodies that neutralize diverse strains of HIV-1. Nature medicine *24*, 857-867.

Yang, L., Sharma, S.K., Cottrell, C., Guenaga, J., Tran, K., Wilson, R., Behrens, A.J., Crispin, M., de Val, N., and Wyatt, R.T. (2018). Structure-Guided Redesign Improves NFL HIV Env Trimer Integrity and Identifies an Inter-Protomer Disulfide Permitting Post-Expression Cleavage. Frontiers in immunology *9*, 1631.

Ye, J., Ma, N., Madden, T.L., and Ostell, J.M. (2013). IgBLAST: an immunoglobulin variable domain sequence analysis tool. Nucleic Acids Res *41*, W34-40.

Yuan, M., Cottrell, C.A., Ozorowski, G., van Gils, M.J., Kumar, S., Wu, N.C., Sarkar, A., Torres, J.L., de Val, N., Copps, J.*, et al.* (2019). Conformational Plasticity in the HIV-1 Fusion Peptide Facilitates Recognition by Broadly Neutralizing Antibodies. Cell Host Microbe *25*, 873-883 e875.

Zhang, K. (2016). Gctf: Real-time CTF determination and correction. Journal of structural biology *193*, 1-12.

Zheng, S.Q., Palovcak, E., Armache, J.P., Verba, K.A., Cheng, Y., and Agard, D.A. (2017). MotionCor2: anisotropic correction of beam-induced motion for improved cryo-electron microscopy. Nature methods *14*, 331-332.

Zimin, A.V., Cornish, A.S., Maudhoo, M.D., Gibbs, R.M., Zhang, X., Pandey, S., Meehan, D.T., Wipfler, K., Bosinger, S.E., Johnson, Z.P.*, et al.* (2014). A new rhesus macaque assembly and annotation for next-generation sequencing analyses. Biol Direct *9*, 20.

Zivanov, J., Nakane, T., Forsberg, B.O., Kimanius, D., Hagen, W.J., Lindahl, E., and Scheres, S.H. (2018). New tools for automated high-resolution cryo-EM structure determination in RELION-3. eLife *7*.

A

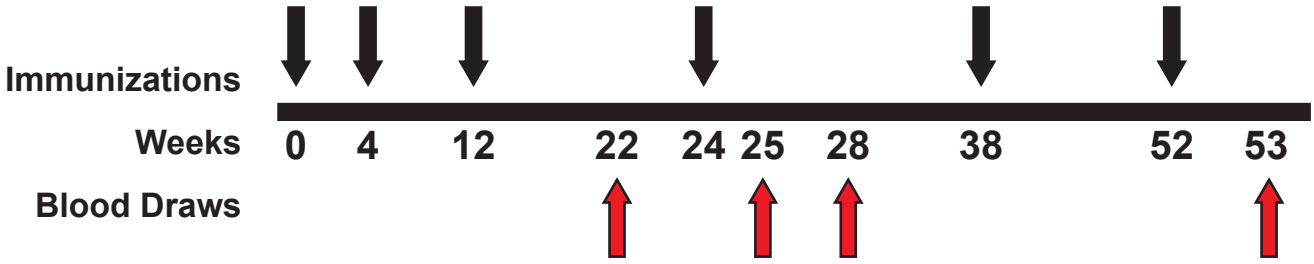

B

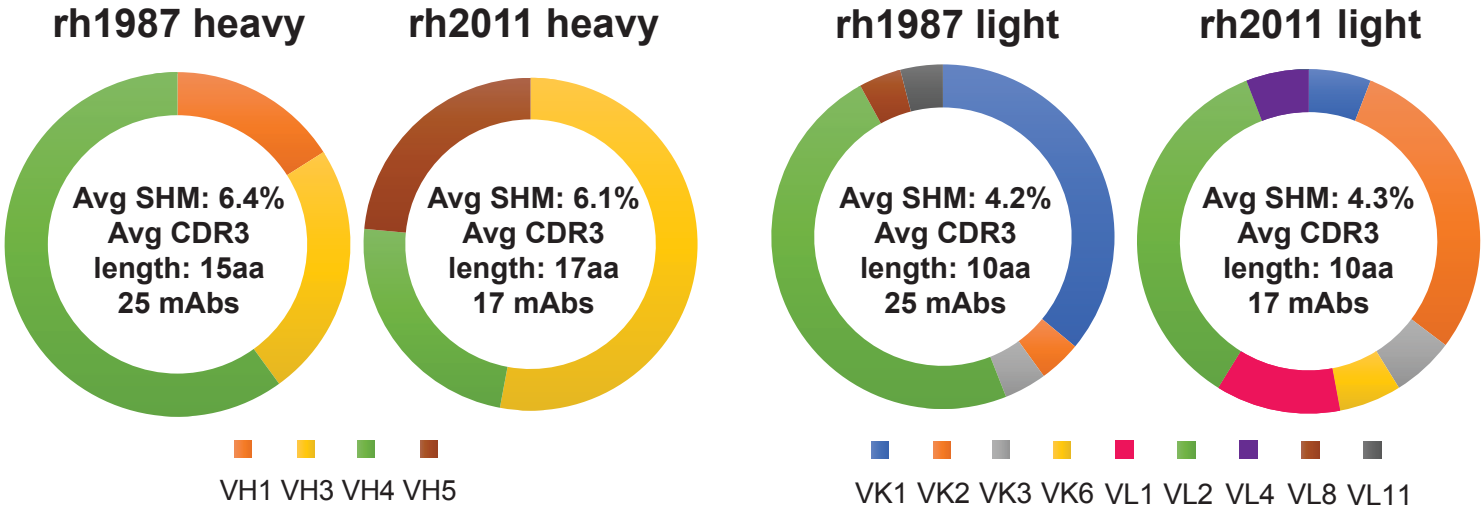

C

rh1987

mAb	BG505 T332N	BG505 T332N+N611A	SF162
RM19A	41.8	>50	>50
RM19A1	44.9	>50	>50
RM19A2	>50	>50	>50
RM19A3	>50	>50	>50
RM19B1	>50	>50	>50
RM19C3	>50	>50	>50
RM19C4	>50	>50	>50
RM19D	>50	>50	>50
RM19J	>50	>50	>50
RM19M	12.9	5.63	>50
RM19N	>50	>50	>50
RM19O	>50	25.5	>50
RM19P	23.5	>50	>50
RM19R	>50	>50	>50
RM19S	>50	3.51	>50
RM19T	>50	>50	>50

IC_{50} (µg/mL)

D

rh2011

mAb	BG505 T332N	BG505 T332N+N611A	SF162
RM20A3	>50	>50	>50
RM20B	>50	>50	>50
RM20C	>50	>50	>50
RM20D	>50	>50	>50
RM20E	>50	<0.41	>50
RM20E1	>50	<0.41	>50
RM20E2	>50	<0.41	>50
RM20E3	>50	<0.41	>50
RM20F	1.6	<0.41	>50
RM20H	42.9	<0.41	>50
RM20I	>50	>50	>50
RM20J	>50	>50	>50

IC_{50} (µg/mL)

A

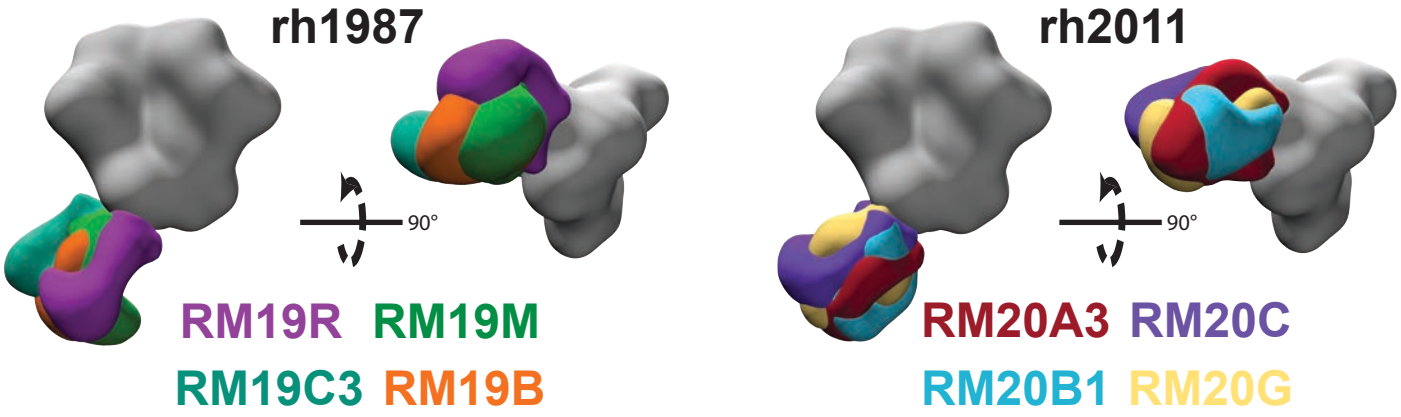

B

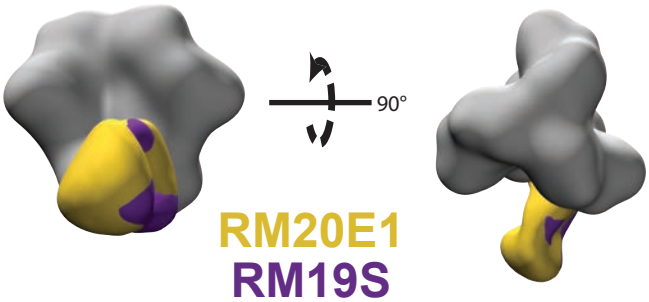

C

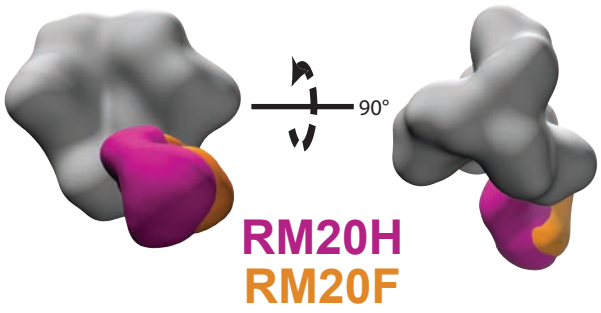

D

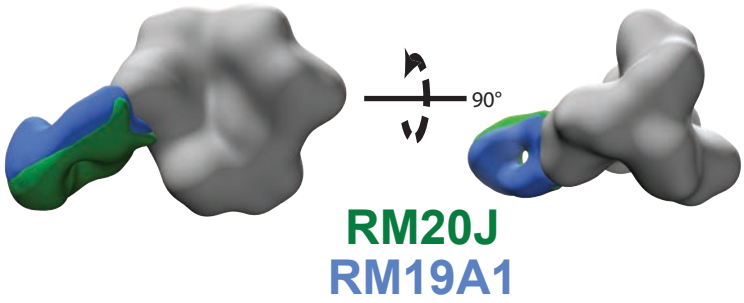

E

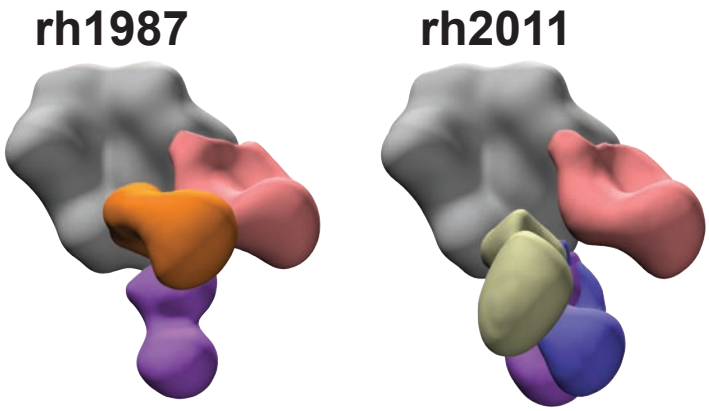

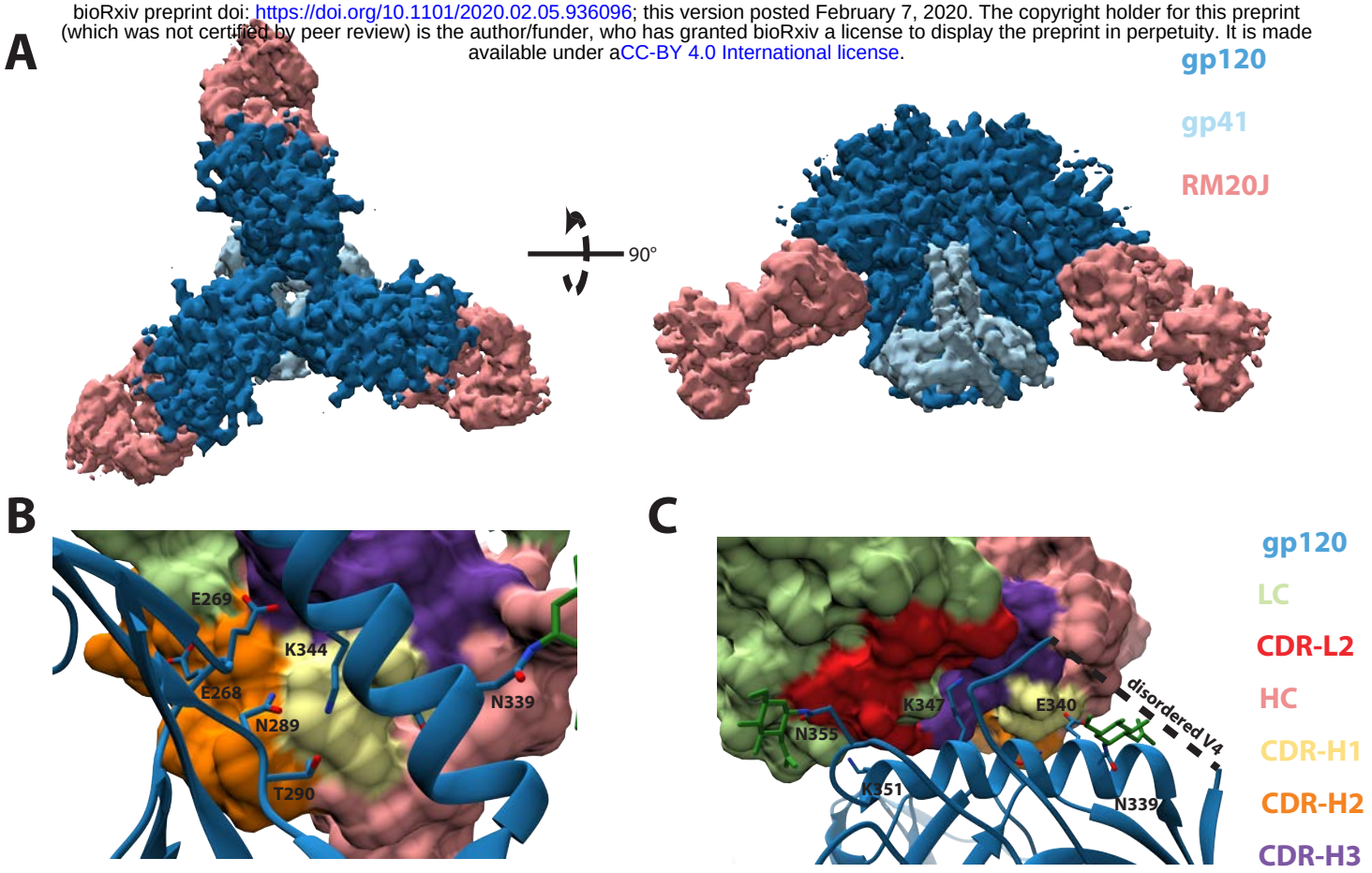

A

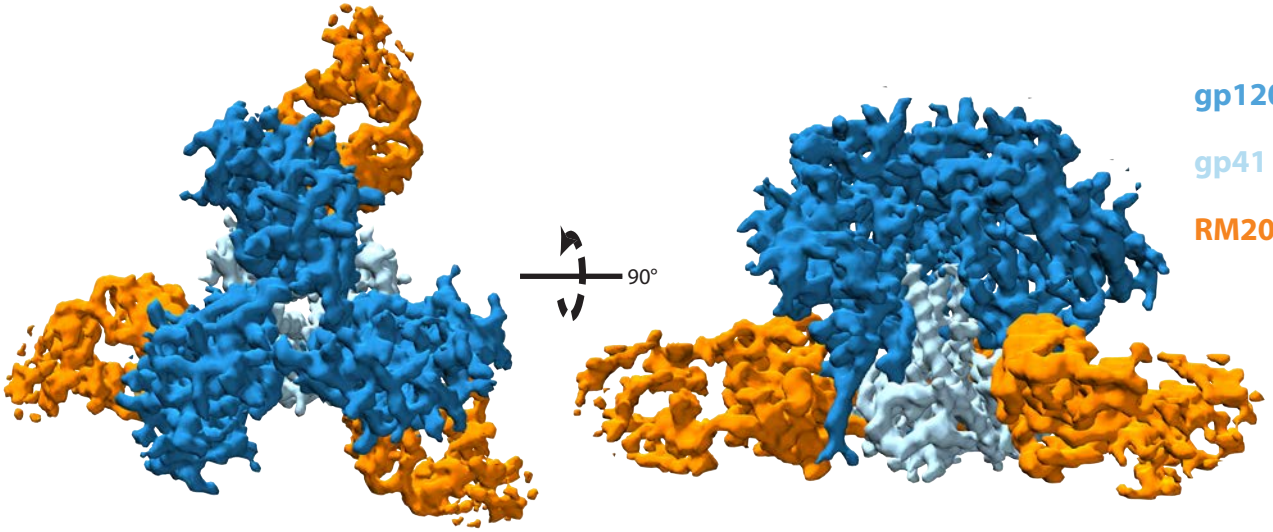

B

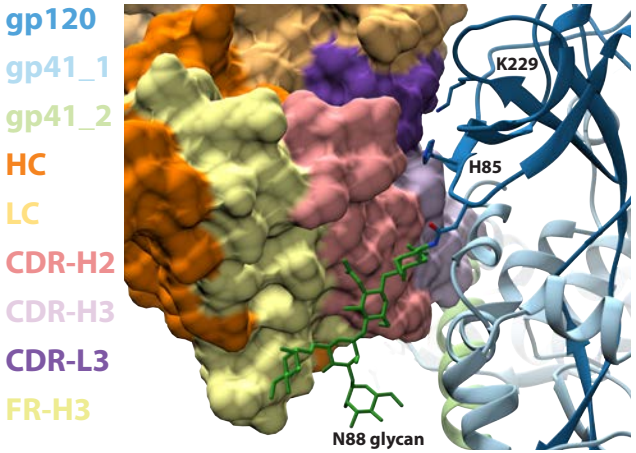

C

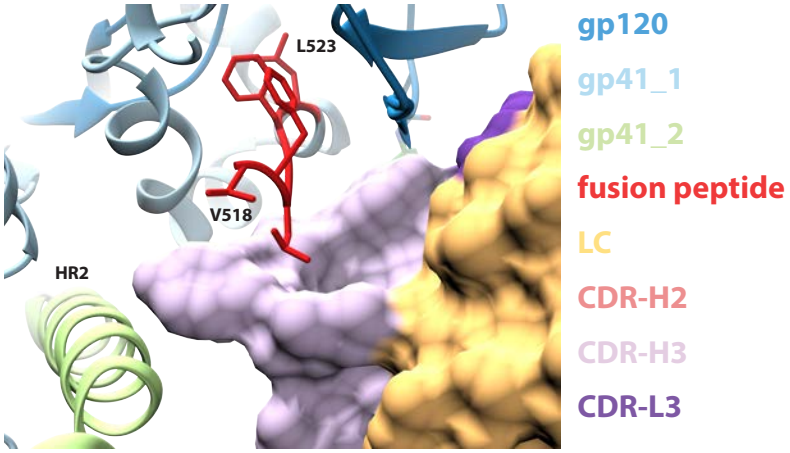

D

	VRC01	RM20F	VRC34
WT	1.0	1.0	1.0
H85A	1.2	11.9	4.7
E87A	1.2	4.3	0.8
N88A	1	>28	>24
K229A	0.6	3.1	1.2
S241N	1.1	6.6	n.d.
E267A	0.8	1.3	0.9
P291T	1.1	2.9	n.d.
N332T	0.9	0.5	n.d.
F522A	0.8	3.9	1.0
M535A	0.9	2.9	1.0
T536A	0.8	2.9	1.5
T538A	0.8	3.6	1.2
N611Q	1.5	<0.1	n.d.
N625Q	1.9	0.6	n.d.
N637Q	1.6	1.2	n.d.
G644A	1.0	4.2	1.8
E647A	1.7	13.5	0.6

fold reduction in neutralization

A

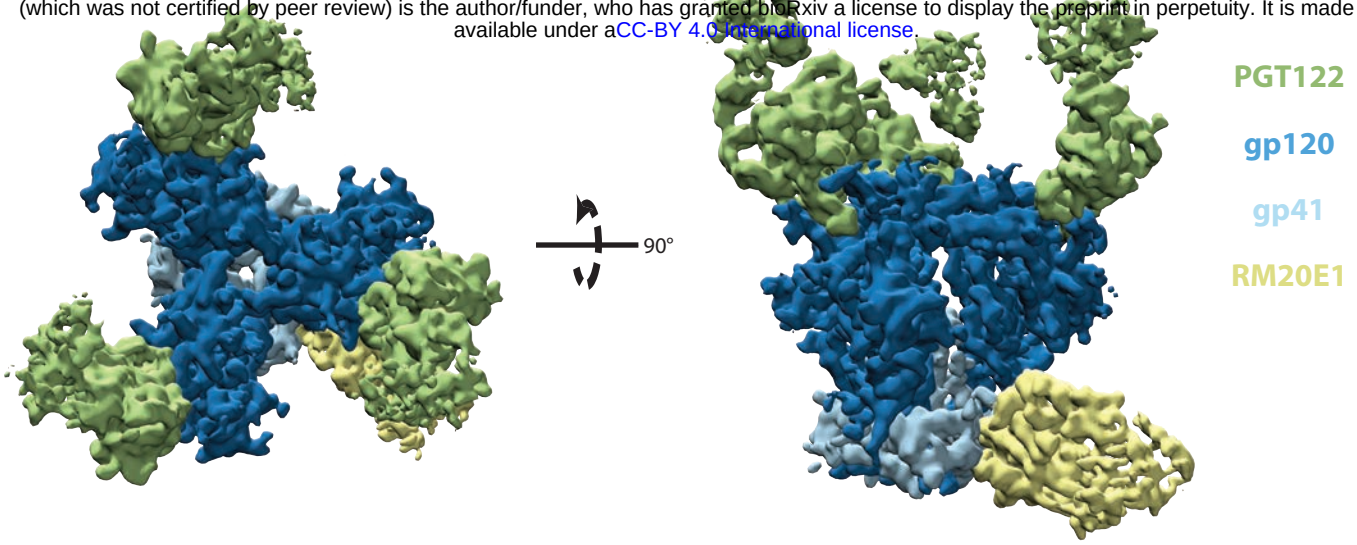

B

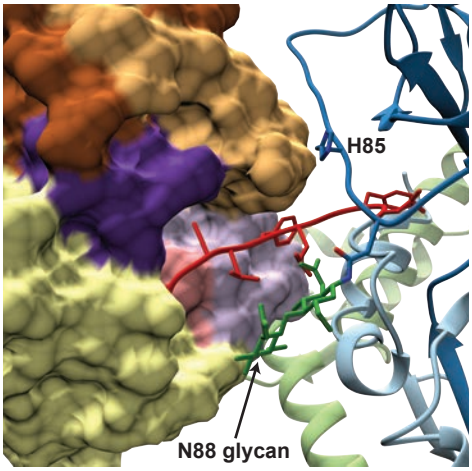

C

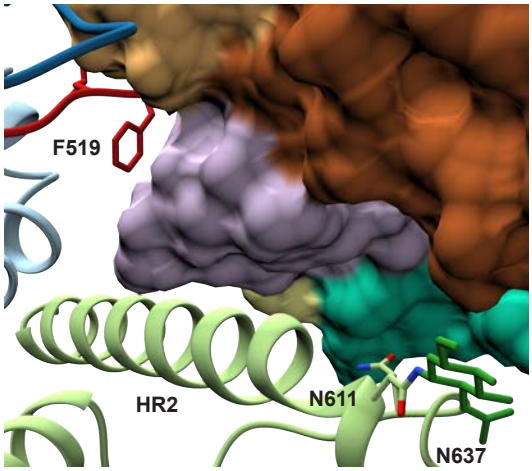

D